

---

# Ancient TL

www.ancienttl.org · ISSN: 2693-0935

---

Issue 32(2) - December 2014

<https://doi.org/10.26034/la.atl.v32.i2>

This issue is published under a Creative Commons Attribution 4.0 International (CC BY):

<https://creativecommons.org/licenses/by/4.0>



© Ancient TL, 2014

# Ancient TL

A periodical devoted to Luminescence and ESR dating

Department of Geography and Earth Sciences, Aberystwyth  
University, Ceredigion SY23 3DB, United Kingdom

and

Department of Physics, East Carolina University  
1000 East 5th Street, Greenville, NC 27858, USA

**Volume 32 No.2**

**December 2014**

**A simple Bayesian method for assessing the standard error of  
equivalent dose estimates**

J. Peng, Z. B. Dong \_\_\_\_\_ 17

**What to do when carbonate replaced water: *Carb*, the model for  
estimating the dose rate of carbonate-rich samples**

B. Mauz, D. Hoffmann \_\_\_\_\_ 24

**Thesis abstracts** \_\_\_\_\_ 33

**Bibliography** \_\_\_\_\_ 42

**Announcements**

XIX INQUA, Nagoya \_\_\_\_\_ 53

ISSN 0735-1348

# Ancient TL

Started by the late David Zimmerman in 1977

---

## EDITOR

**G.A.T. Duller**, Department of Geography and Earth Sciences, Aberystwyth University, Ceredigion SY23 3DB, United Kingdom ([ggd@aber.ac.uk](mailto:ggd@aber.ac.uk))

and

**R.DeWitt**, Department of Physics, East Carolina University, Howell Science Complex, 1000 E. 5th Street Greenville, NC 27858, USA ([dewittr@ecu.edu](mailto:dewittr@ecu.edu))

## EDITORIAL BOARD

**I.K. Bailiff**, Luminescence Dosimetry Laboratory, Dawson Building, University of Durham, South Road, Durham DH1 3LE, United Kingdom ([ian.bailiff@durham.ac.uk](mailto:ian.bailiff@durham.ac.uk))

**S.H. Li**, Department of Earth Sciences, The University of Hong Kong, Hong Kong, China ([shli@hku.hk](mailto:shli@hku.hk))

**R.G. Roberts**, School of Geosciences, University of Wollongong, Wollongong, NSW 2522, Australia ([rgrob@uow.edu.au](mailto:rgrob@uow.edu.au))

---

## REVIEWERS PANEL

**R.M. Bailey**, Oxford University Centre for the Environment, Dyson Perrins Building, South Parks Road, Oxford OX1 3QY, United Kingdom ([richard.bailey@ouce.ox.ac.uk](mailto:richard.bailey@ouce.ox.ac.uk))

**J. Faïn**, Laboratoire de Physique Corpusculaire, 63177 Aubière Cedex, France ([jean.fain@wanadoo.fr](mailto:jean.fain@wanadoo.fr))

**R. Grün**, Research School of Earth Sciences, Australian National University, Canberra ACT 0200, Australia ([rainer.grun@anu.edu.au](mailto:rainer.grun@anu.edu.au))

**T. Hashimoto**, Department of Chemistry, Faculty of Sciences, Niigata University, Niigata 950-21, Japan ([thashi@curie.sc.niigata-u.ac.jp](mailto:thashi@curie.sc.niigata-u.ac.jp))

**D.J. Huntley**, Department of Physics, Simon Fraser University, Burnaby B.C. V5A1S6, Canada ([huntley@sfu.ca](mailto:huntley@sfu.ca))

**M. Lamothe**, Dépt. Sci. de la Terre, Université du Québec à Montréal, CP 8888, H3C 3P8, Montréal, Québec, Canada ([lamothe.michel@uqam.ca](mailto:lamothe.michel@uqam.ca))

**N. Mercier**, Lab. Sci. du Climat et de l'Environ, CNRS-CEA, Av. de la Terrasse, 91198, Gif sur Yvette Cedex, France ([norbert.mercier@lscce.cnrs-gif.fr](mailto:norbert.mercier@lscce.cnrs-gif.fr))

**D. Miallier**, Laboratoire de Physique Corpusculaire, 63177 Aubière Cedex, France ([miallier@clermont.in2p3.fr](mailto:miallier@clermont.in2p3.fr))

**S.W.S. McKeever**, Department of Physics, Oklahoma State University, Stillwater Oklahoma 74078, U.S.A. ([stephen.mckeever@okstate.edu](mailto:stephen.mckeever@okstate.edu))

**A.S. Murray**, Nordic Laboratory for Luminescence Dating, Risø National Laboratory, Roskilde, DK-4000, Denmark ([andrew.murray@risoe.dk](mailto:andrew.murray@risoe.dk))

**N. Porat**, Geological Survey of Israel, 30 Malkhe Israel St., Jerusalem 95501, Israel ([naomi.porat@gsi.gov.il](mailto:naomi.porat@gsi.gov.il))

**D. Richter**, Lehrstuhl Geomorphologie, University of Bayreuth, 95440 Bayreuth, Germany ([daniel.richter@uni-bayreuth.de](mailto:daniel.richter@uni-bayreuth.de))

**D.C.W. Sanderson**, Scottish Universities Environmental Research Centre, Scottish Enterprise Technology Park, East Kilbride G75 0QF, UK ([David.Sanderson@glasgow.ac.uk](mailto:David.Sanderson@glasgow.ac.uk))

**A.K. Singhvi**, Rm 203, Physical Research Laboratory, Navrangpura, Ahmedabad 380009, India ([singhvi@prl.res.in](mailto:singhvi@prl.res.in))

**K.J. Thomsen**, Radiation Research Division, Risø National Laboratory for Sustainable Energy, Technical University of Denmark, DK-4000, Roskilde, Denmark ([krth@risoe.dtu.dk](mailto:krth@risoe.dtu.dk))

---

# Ancient TL

A periodical devoted to Luminescence and ESR dating

Web site: <http://www.aber.ac.uk/ancient-tl>

will move to: <http://www.ecu.edu/cs-cas/physics/Ancient-TL.cfm>

Department of Geography and Earth Sciences  
Aberystwyth University SY23 3DB  
United Kingdom

Tel: (44) 1970 622606      Fax: (44) 1970 622659      E-mail: [ggd@aber.ac.uk](mailto:ggd@aber.ac.uk)

future address and contact:

Department of Physics, East Carolina University  
Greenville, NC 27858, USA

Tel: +252-328-4980      Fax: +252-328-0753      E-mail: [dewittr@ecu.edu](mailto:dewittr@ecu.edu)



# A simple Bayesian method for assessing the standard error of equivalent dose estimates

Jun Peng, ZhiBao Dong

Cold and Arid Regions Environmental and Engineering Research Institute, Chinese Academy of Sciences, 730000 Lanzhou, China

\*Corresponding author: pengjun10@mails.ucas.ac.cn

(Received 8 August 2014; in final form 17 November 2014)

## Abstract

Estimating the equivalent dose (ED) value is critical to obtaining the burial dose for Optically Stimulated Luminescence (OSL) dating. In this study, a simple Bayesian method is used to assess the standard error of an ED value in a linear or an exponential model. An ED value is treated as a stochastic node that depends on a random variable whose posterior distribution can be constructed and sampled. The results show that the Bayesian approach may improve the precision of an ED estimate by avoiding the repeated curve-fitting procedure employed in the routine “parametric bootstrap” Monte Carlo method.

**Key words:** Bayesian method; Markov chain Monte Carlo; equivalent dose; standard error

## Introduction

In the commonly adopted single aliquot regenerative-dose (SAR) protocol (Murray and Wintle, 2000; Murray and Wintle, 2003), the standardized natural OSL signal is projected onto the growth curve that is constructed using a series of sensitivity-corrected regenerative OSL signals to calculate the corresponding ED value. A maximum likelihood method was used by Yoshida et al. (2000) to fit the growth curve with an exponential-plus-linear model in which the true ED value was treated as an unknown parameter, and the standard error of the ED value was estimated through the profile likelihood function. However, this method may result in unreliable estimates (Yoshida et al., 2003) as the number of points is not many more than the dimension of the problem under consideration (Galbraith and Roberts, 2012). This problem led Yoshida et al. (2003) to use a “parametric bootstrap” method to simulate and fit a number of growth curves repeatedly to obtain a more reliable estimate of the standard error of an ED value. Duller (2007a) gave a detailed introduction about how to estimate an ED

value and outlined two protocols (i.e. simple transformation and Monte Carlo simulation) to assess its standard error. Berger (2010) outlined methods that incorporate the contribution of errors from the characteristic parameters of a growth curve and their covariances to estimate standard errors of ED values. Classic numeric techniques such as non-linear parameter optimization and interpolation are routinely employed in these procedures (Peng et al., 2013). In this study, a simple Bayesian method was constructed to estimate ED values and their standard errors using measured datasets. The Gibbs sampler *WinBUGS* (Lunn et al., 2013) was employed to perform the Bayesian Markov chain Monte Carlo sampling, and the estimates were compared to those assessed using the *Analyst* software (Duller, 2007b).

## Methods

We use  $x_i$  and  $y_i$  to denote the  $i$ -th regenerative dose and measured standardized (i.e. sensitivity corrected) OSL, respectively, for each of the  $i=1$  to  $n$  observations. A saturating exponential growth curve may be described as:

$$\hat{y}_i = a(1 - e^{-bx_i}) + c \quad (\text{Eqn. 1})$$

where  $\hat{y}_i$  denotes the  $i$ -th fitted standardized OSL and  $a, b, c$  are parameters to be optimized. Here  $a$  is the saturation level (maximum value) of the standardized OSL,  $b$  is the reciprocal of the saturation dose, and  $c$  is an offset accounting for potential “recuperation” effects. Let  $y_0$  and  $x_0$  denote the natural standardized OSL and the corresponding ED value respectively. An estimate of the ED value can be obtained by inverting Eqn. 1 analytically:

$$x_0 = -\frac{\ln[(a - y_0 + c)/a]}{b} \quad (\text{Eqn. 2})$$

Eqn. 2 is justified only if  $a + c > y_0$ , that is, the natural standardized OSL  $y_0$  must not exceed the saturation level of the growth curve. It should be noted that even if the natural standardized OSL  $y_0$  is close to (but does not exceed) the saturation level, the randomly selected quantity  $Y_0 \sim N(y_0, \sigma_0)$  (see below) may exceed the maximum due to random errors controlled by its standard error  $\sigma_0$ . For this reason, it is best to ensure that the dose to be estimated does not exceed the double value of the saturation dose (Wintle and Murray, 2006).

Software *Analyst* (Duller, 2007b) employs the Levenberg-Marquardt algorithm to estimate the parameters of a saturating exponential growth curve. Once the parameters are determined, an ED value can be calculated with Eqn. 2 or an interpolation procedure using the natural standardized OSL. The “parametric bootstrap” Monte Carlo method that assesses the standard error of the ED value involves fitting the growth curve and calculating the ED value repeatedly using random natural and regenerative standardized OSL signals simulated from normal distributions whose widths are determined by the relevant standard deviations (see Duller, 2007a for details). In the following part, we derive a simple alternative that avoids the repeated fitting process needed in the routine Monte Carlo procedure for obtaining the sampling distribution of an ED value of a saturating exponential growth curve using the Bayesian approach. The ED value whose distribution is determined is treated as a stochastic node that depends on parameters whose sampling distributions can be simulated via a Markov chain Monte Carlo method.

Firstly, note that it is possible to reduce the dimension of the problem under consideration to contain only parameter  $b$  via a linear algebraic method (Peng et al., 2013), just as that used in deconvolution of decay curves in previous studies (Bluszcz, 1996; Bluszcz and Adamiec, 2006). Let  $w_i$  be the weight of  $y_i$ . For a number of observations and a given  $b$  value, parameter  $a$  can be calculated as:

$$a = \frac{\sum_{i=1}^n w_i \sum_{i=1}^n w_i (1 - e^{-bx_i}) y_i - \sum_{i=1}^n w_i (1 - e^{-bx_i}) \sum_{i=1}^n w_i y_i}{\sum_{i=1}^n w_i \sum_{i=1}^n w_i (1 - e^{-bx_i})^2 - [\sum_{i=1}^n w_i (1 - e^{-bx_i})]^2} \tag{Eqn. 3}$$

Similarly, parameter  $c$  can be determined by:

$$c = \frac{\sum_{i=1}^n w_i y_i - a \sum_{i=1}^n w_i (1 - e^{-bx_i})}{\sum_{i=1}^n w_i} \tag{Eqn. 4}$$

In a weighted nonlinear least-squares estimation we wish to minimize  $\chi^2 = \sum w_i (y_i - \hat{y}_i)^2$ , where the weight  $w_i$  are equal to  $1 / \sigma_i^2$ . The estimates obtained with a least-squares estimation will be identical to those given by a maximum likelihood estimation if we suppose that each of the  $i$ -th regenerative standardized OSL is independent of the others and follows a normal distribution with mean  $\hat{y}_i$  and standard error  $\sigma_i$ , i.e.,  $y_i \sim N(\hat{y}_i, \sigma_i)$ . Note that  $\hat{y}_i$  is the model based (fitted) standardized OSL and  $\sigma_i$  is the standard error (based on photon counting statistics and measurement error) for the measured  $y_i$ . Combining Eqn. 1, 3 and 4, we can treat  $\hat{y}_i$  as a function of the observations  $(x_i, y_i, w_i)$  and parameter  $b$ , which we denote as  $\hat{y}_i = F(x_i, y_i, w_i, b)$ .  $prob(x, y, w | b)$  is the probability for observing the standardized OSL signals  $y$  with fixed weights  $w$  at doses  $x$  if the reciprocal saturation dose has the value of  $b$ , it can be written as:

$$prob(x, y, w | b) = \prod_{i=1}^n \frac{\sqrt{w_i}}{\sqrt{2\pi}} e^{-\frac{w_i (y_i - F(x_i, y_i, w_i, b))^2}{2}} \tag{Eqn. 5}$$

Similar to Eqn. 5,  $prob(b|x,y,w)$  is the probability that  $b$  has a given value if the observations are  $x,y,w$ , and it is called the posterior distribution of  $b$ . From Eqn. 1-5, it can be seen that if one is able to simulate a random variable  $b$  based on its posterior distribution, then variables  $a, c, x_0$  can be regarded as stochastic nodes that depend on the value of  $b$ . According to Bayes’ theorem (Sivia, 1996), the posterior distribution of  $b$  under condition of the observed values is:

$$prob(b | x, y, w) \propto prob(x, y, w | b) prob(b) \tag{Eqn. 6}$$

$prob(b)$  is the so-called prior of  $b$ , and if it follows a uniform distribution (i.e.  $prob(b)$  is a constant), then sampling a random variable  $b$  from its posterior distribution is equal to sampling a  $b$  value according to the joint-likelihood function determined by Eqn. 5. A good choice for the prior of  $b$  is the uniform distribution  $U(0,1)$ , which is equal to 1 for all values of  $b$  between 0 and 1, and 0 for all other values.

This simulation can be easily performed with a general Markov chain Monte Carlo sampler, in our case the software *WinBUGS* (Lunn et al., 2013). *WinBUGS* requires as input (1) the measured values  $(x, y, w)$ , (2) the model (i.e. Eqn. 1), (3) the prior distribution for the parameter to be simulated, in our case  $U(0,1)$  for parameter  $b$ , (4) Eqn. 3-4 to reduce the dimension of the model, and (5) Eqn. 2 to allow calculation of the node  $x_0$ . The software creates automatically a random  $b$  value according to Eqn. 5. Parameters  $a$ ,  $c$  depend on the value of  $b$  (see Eqn. 3-4). They are the by-product of the simulation and are regarded as nodes. By using randomly generated natural standardized OSL values  $Y_0 \sim N(y_0, \sigma_0)$  and the nodes  $a$  and  $c$ , the sampling distribution of ED values (i.e.  $x_0$ ) can be monitored according to Eqn. 2. That means the distributions of these quantities can be obtained iteratively, i.e. each time a value of  $b$  is generated and the values of  $a$  and  $c$  are calculated, and the value of the ED can be monitored. After a large number of simulations, we can infer statistical quantities such as the mean, the median, the standard deviation, and the 95% confidence interval of these parameters. There are certain benefits to reduce the dimension of the problem to contain only one independent variable. Firstly, this makes the posterior distribution of  $b$  be mainly dominated by the likelihood function and the prior is almost irrelevant, as a number of data points are used to simulate only one parameter. Another advantage of reducing the dimension lies in that it facilitates the sampling process. The Gibbs sampler may fail to converge and the generated samples may have poor mixing properties if there are many quantities that need to be sampled, as parameters in this model are highly correlated with each other.

The same methodology would apply to a linear growth curve by setting the slope as the independent variable and treating the intercept and ED value as nodes that depend on the value of the slope. Also, the procedure may be modified to apply to a quadratic growth curve. However, this method is inapplicable to an exponential plus linear model, as this model cannot be inverted analytically as  $x = f^{-1}(y)$  and software *WinBUGS* does not have a standard function to do interpolation of this kind.

### Results of Comparisons and Discussions

Measured datasets from 35 aliquots of samples GL1-1 and 36 aliquots of sample GL1-2 (Peng and Han, 2013) were analyzed. Decay curves of these two samples have variable OSL intensities (Peng et al., 2014). The net OSL intensity was calculated using integration of the first 0.64s after subtracting background from the last 50 channels in a decay curve. The standard error of the sensitivity-corrected OSL was based on counting statistics and a

measurement error of 2%. Datasets from sample GL1-1 and GL1-2 were fitted with a saturating exponential and a linear growth curve, respectively. We compared the estimates derived from the Bayesian method outlined above using software *WinBUGS* (version 1.4.3) with the results of the “parametric bootstrap” Monte Carlo method described by Duller (2007a) using software *Analyst* (version 4.12). Software *WinBUGS* was called in batch mode via the package *R2WinBUGS* (version 2.1-19) (Sturtz et al., 2005) for the *R* statistical software so that datasets can be easily loaded and analyzed. The outputs are summary statistics (the mean, the standard deviation, the 95% confidence interval, etc.) for the relevant parameters of the growth curve and the desired ED value. Scripts for running the models are presented in the supplementary. In software *Analyst*, the number of Monte Carlo iterations was set equal to 1,000. In software *WinBUGS*, each dataset was simulated through 50,000 iterations and the posterior inference was based on 8,000 iterations. As is common procedure with these types of simulations the initial 10,000 iterations were discarded (“burn-in”) and every 5-th iteration was retained (“thinning”). The kernel density plots of the parameters derived from the exponential model simulation for an aliquot of sample GL1-1 are shown in Figure 1. Related trace plots of the variations of parameters and ED value with the number of iterations are shown in Figure 2. The unimodal and symmetric distribution pattern (Figure 1) and good mixing property (Figure 2) demonstrated in the simulated  $b$  value (also shown in the ED value) indicate that the simulation appears to converge. To test the program we also attempted to fit an exponential model to a number of linear growth curves. Our analysis suggests that for a growth curve that is linear or approximately linear, the sampling distribution of the saturating OSL (i.e. parameter  $a$ ) may seem to be very inhomogeneous and highly variable if an exponential model is applied. But even in this case, the posterior of  $b$  and the resultant ED values can still converge to a unimodal distribution.

Figure 3 (A-B) shows a linear growth curve for an aliquot of sample GL1-2 and an exponential growth curve for an aliquot of sample GL1-1 that are fitted using the Bayesian approach. A comparison of ED values and their standard errors estimated using the “parametric bootstrap” Monte Carlo method and the simple Bayesian method is presented in Figure 3 (C-F). A paired two-tailed t-test with a 1% significance level is used to test the significance of difference between the results of the two methods. For datasets from sample GL1-1 that are fitted with an exponential model, the t-values calculated using the difference of ED values and the difference of errors of ED values are 0.16 and 5.06, respectively,

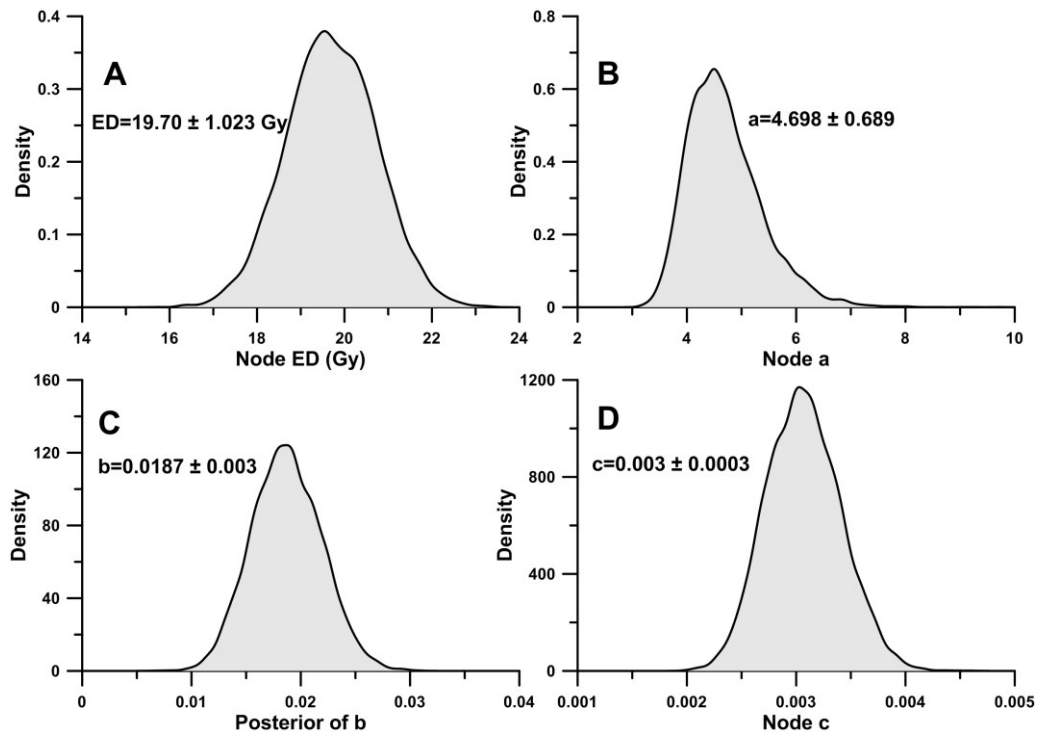


**Figure 1:** Kernel density plots for the ED value and characteristic parameters of a saturating exponential growth curve using an aliquot from sample GL1-1. Each plot is drawn using 8,000 samples. The plots show unimodal distributions. Note: The density values plotted on the y-axis should not be confused with probability distributions and can have values larger than 1.

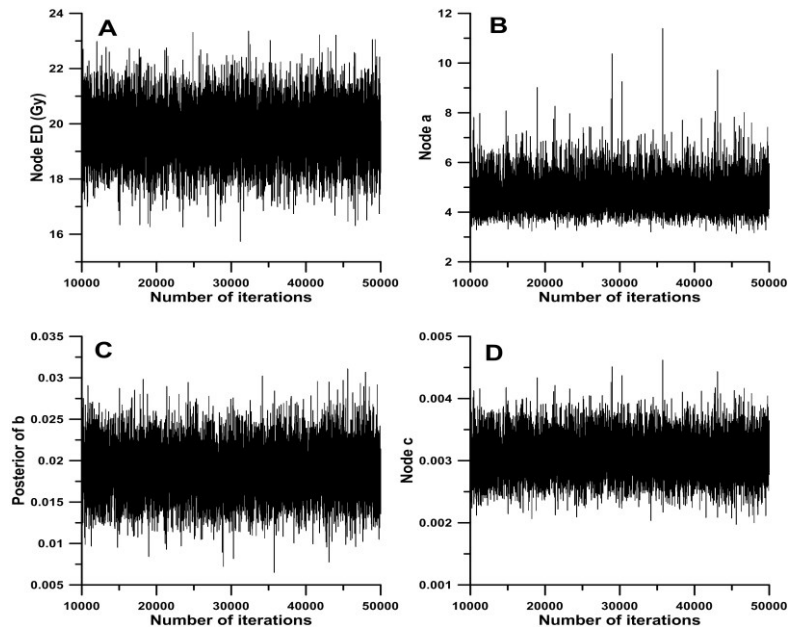


**Figure 2:** Variations of simulated ED values and characteristic parameters with the number of iterations in an exponential model for an aliquot from sample GL1-1. Each plot is drawn using 8,000 samples. Throughout the simulation variables are evenly spread over their feasible spaces, reflecting good mixing properties.

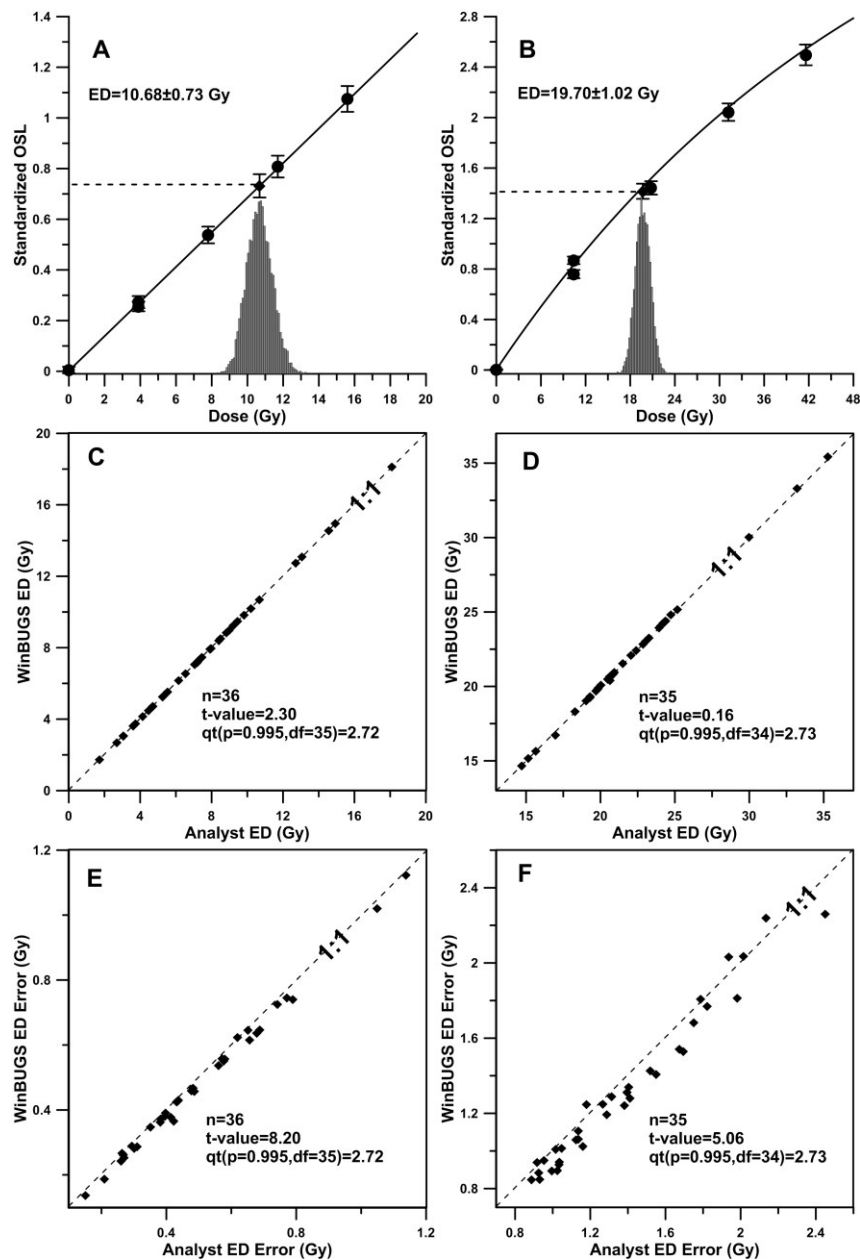


**Figure 3:** A linear growth curve for an aliquot of sample GL1-2 (A) and an exponential growth curve for an aliquot of sample GL1-1 (B) that are fitted using the Bayesian method. C and D: Comparisons of ED values obtained using the Monte Carlo method and the Bayesian method for samples GL1-2 and GL1-1, respectively. E and F: Comparisons of standard errors of ED values assessed using the Monte Carlo method and the Bayesian method for samples GL1-2 and GL1-1, respectively.

and the critical t-value is 2.73. This demonstrates that there is no significant difference between the two sets of ED values, but there are obvious differences between the standard errors at a significance level of 1%. Similar results are found in estimates from sample GL1-2 that have a theory t-value of 2.72. ED values estimated using the two different methods are

comparable, though the ED value estimated by software *Analyst* is based on solely the natural standardized OSL while the ED value obtained from the Bayesian method is the mean value of all resulting samples in node ED. This consistency may result from the fact that software *Analyst* assigns unequal weights to the observations using inverse

variances so the shape of the resultant growth curve is akin to that fitted by a maximum likelihood estimation using Eqn. 5. However, it turned out that for the analyzed aliquots almost all standard errors of ED values assessed by the Bayesian method using software *WinBUGS* are smaller than that estimated by the “parametric bootstrap” Monte Carlo method using software *Analyst*, though in general the differences are small. The uncertainties arising from photon counting statistics (Galbraith, 2002; Li, 2007; Adamiec et al., 2012; Galbraith, 2014), the instrument reproducibility (Truscott et al., 2000; Thomsen et al., 2005), and the growth-curve fitting error (Jacobs et al., 2006; Duller, 2007a) are the three major source of uncertainties involved in estimating an ED value. The differences of errors between the two methods cannot be caused by the first two sources of error that influence the uncertainty of the standardized OSL if the same dataset is analyzed. For a Monte Carlo method in which growth curves are simulated and fitted repeatedly, bias is introduced in each iteration. But the Bayesian method in which the ED value is treated as a node that depends on a single variable that can be sampled from its posterior distribution avoids the curve-fitting process and may result in a reduction in the standard error of an ED estimate hence an improvement in precision.

A predominate advantage of the simple Bayesian protocol is that a user need not pay much attention to the initialization of parameters, unlike that encountered when applying a classic nonlinear method (Peng et al., 2013). Another benefit of the Bayesian method is the flexibility with which posterior inferences can be summarized (Gelman et al., 2013). The Bayesian approach outlined above can be modified to be more flexible to obtain more variable ED distributions. McCoy et al. (2000) observed that individual grains of quartz exhibit log-norm distributions in their OSL intensities. Thus a log-norm distribution may be assumed for the standardized OSL (Yoshida et al., 2003) when simulating an ED value. Whether normal or log-normal distributions are assumed will make little difference if the uncertainty of a sensitivity-corrected OSL is relatively small (Galbraith and Roberts, 2012). It is also possible to specify the standardized OSL to have constant relative uncertainty (i.e.  $\sigma_i = ky_i$ ), then the estimate will be equal to that given by a weighted nonlinear least-squares method with weights  $1/y_i^2$  if we ignore the common constant (Thompson, 2007). Moreover, if few outliers are presented in a number of data points, the standardized OSL may be assumed to follow a heavily-tailed distribution (say, the *t*-distribution) so that outliers can be accommodated. Additionally, in all the preceding analysis, we have implicitly assumed that the regenerative dose values are known exactly. But

in fact, this assumption may be far from the truth as the precision of a given dose is instrument-dependent. If the associated error-bars for the x-coordinate are not known, then we may perform the simulation by assuming that they have constant relative uncertainty, say, 1% or 2%, and the resultant ED values will be more variable in this way. However, it should be noted that the sensitivity of the model to the imposed assumptions needs to be carefully checked, and that any conflict between the assumptions and the data may crash the simulation or result in absurd posteriors within a Bayesian framework. It is essentially the user’s responsibility to ensure that the resulting posterior distribution is correct when special priors or assumptions are assumed.

### Conclusion

A simple Bayesian approach is used to estimate ED values and assess their standard errors for a linear and a saturating exponential growth curve. The resulting ED values are comparable to those obtained by a weighted nonlinear least-square fit. This method avoids the repeated curve-fitting procedures required by the “parametric bootstrap” Monte Carlo protocol in error assessments, and may result in an improvement in the precision of an ED value.

### Acknowledgments

We would like to thank Dr Regina DeWitt for improving the language of this manuscript. Comments by Dr Regina Dewitt have substantially improved the manuscript. This work was funded by the Ministry of Science and Technology of the People's Republic of China (2013CB956000).

### References:

- Adamiec, G., Heer, A.J., Bluszcz, A. (2012). Statistics of count numbers from a photomultiplier tube and its implications for error estimation. *Radiation Measurements* 47: 746-751.
- Berger, G.W., 2010. Estimating the error in equivalent dose obtained from SAR. *Ancient TL* 28: 55-66.
- Bluszcz, A. (1996). Exponential function fitting to TL growth data and similar applications. *Geochronometria* 13: 135-141.
- Bluszcz, A., Adamiec, G. (2006). Application of differential evolution to fitting OSL decay curves. *Radiation Measurements* 41: 886-891.
- Duller, G.A.T. (2007a). Assessing the error on equivalent dose estimates derived from single aliquot regenerative dose measurements. *Ancient TL* 25: 15-24.
- Duller, G.A.T. (2007b). *Software Analyst. Manual*, page.1-45.

- [http://www.nutech.dtu.dk/english/Products-and-Services/Dosimetry/Radiation-Measurement-Instruments/TL\\_OSL\\_reader/Software](http://www.nutech.dtu.dk/english/Products-and-Services/Dosimetry/Radiation-Measurement-Instruments/TL_OSL_reader/Software).
- Galbraith, R. F. (2002). A note on the variance of a background-corrected OSL count. *Ancient TL* 20: 49-51.
- Galbraith, R.F. (2014). A further note on the variance of a background-corrected OSL count. *Ancient TL* 32: 1-3.
- Galbraith, R.F., Roberts, R.G. (2012). Statistical aspects of equivalent dose and error calculation and display in OSL dating: An overview and some recommendations. *Quaternary Geochronology* 11: 1-27.
- Gelman, A., Carlin, J. B., Stern, H. S., Dunson, D. B., Vehtari, A., Rubin, D. B. (2013). *Bayesian data analysis*. CRC press.
- Jacobs, Z., Duller, G.A.T., Wintle, A.G. (2006). Interpretation of single grain De distributions and calculation of De. *Radiation Measurements* 41: 264-277.
- Li, B. (2007). A note on estimating the error when subtracting background counts from weak OSL signals. *Ancient TL* 25: 9-14.
- Lunn, D., Jackson, C., Best, N., Thomas, A., Spiegelhalter, D. (2013). *The BUGS book: a practical introduction to Bayesian analysis*. Boca Raton, Florida: CRC Press.  
<http://www.mrc-bsu.cam.ac.uk/software/bugs/>.
- McCoy, D.G., Prescott, J.R., Nation, R.J. (2000). Some aspects of single-grain luminescence dating. *Radiation Measurements* 32: 859-864.
- Murray, A.S., Wintle, A.G. (2000). Luminescence dating of quartz using an improved single-aliquot regenerative-dose protocol. *Radiation Measurements* 32: 57-73.
- Murray, A.S., Wintle, A.G. (2003). The single aliquot regenerative dose protocol: potential for improvements in reliability. *Radiation Measurements* 37: 377-381.
- Peng, J., Dong, Z.B., Han, F.Q., Han, Y.H., Dai, X.L. (2014). Estimating the number of components in an OSL decay curve using the Bayesian Information Criterion. *Geochronometria* 41: 334-341.
- Peng, J., Dong, Z.B., Han, F.Q., Long, H., Liu, X.J. (2013). R package numOSL: numeric routines for optically stimulated luminescence dating. *Ancient TL* 31: 41-48. <http://CRAN.R-project.org/package=numOSL>.
- Peng, J., Han, F.Q. (2013). Selections of Fast-component OSL Signal Using Sediments from the South Edge of Tengger Desert. *Acta Geoscientica Sinica* 34: 757-762 (in Chinese with English abstract).
- Sivia, D.S. (1996). *Data analysis: a Bayesian tutorial*. Oxford University Press, Oxford.
- Sturtz, S., Ligges, U., Gelman, A. (2005). R2WinBUGS: A package for running WinBUGS from R. *Journal of statistical software* 12: 1-16. <http://CRAN.R-project.org/package=R2WinBUGS>.
- Thompson, J.W. (2007). Accuracy, precision, and irradiation time for Monte Carlo simulations of single aliquot regeneration (SAR) optically stimulated luminescence (OSL) dosimetry measurements. *Radiation Measurements* 42:1637-1646.
- Thomsen, K.J., Murray, A.S., Bøtter-Jensen, L. (2005). Sources of variability in OSL dose measurements using single grains of quartz. *Radiation Measurements* 39: 47-61.
- Truscott, A.J., Duller, G.A.T., Bøtter-Jensen, L., Murray, A.S., Wintle, A.G. (2000). Reproducibility of optically stimulated luminescence measurements from single grains of Al<sub>2</sub>O<sub>3</sub>:C and annealed quartz. *Radiation Measurements* 32: 447-451.
- Wintle, A.G., Murray, A.S. (2006). A review of quartz optically stimulated luminescence characteristics and their relevance in single-aliquot regeneration dating protocols. *Radiation Measurements* 41: 369-391.
- Yoshida, H., Roberts, R.G., Olley, J.M., Laslett, G.M., Galbraith, R.F. (2000). Extending the age range of optical dating using single 'supergrains' of quartz. *Radiation Measurements* 32: 439-446.
- Yoshida, H., Roberts, R.G., Olley, J.M. (2003). Progress towards single-grain optical dating of fossil mud-wasp nests and associated rock art in northern Australia. *Quaternary Science Reviews* 22: 1273-1278.

**Reviewer**  
R. DeWitt

# What to do when carbonate replaced water: *Carb*, the model for estimating the dose rate of carbonate-rich samples

Barbara Mauz<sup>1</sup> and Dirk Hoffmann<sup>2</sup>

<sup>1</sup>School of Environmental Sciences, University of Liverpool, Jane Herdman Building, Liverpool L69 3GP, United Kingdom

<sup>2</sup>School of Geographical Sciences, University of Bristol, University Road, Bristol BS8 1SS United Kingdom

(Received 4 September 2014; in final form 21 November 2014)

## Introduction

In 2008 we published a paper (Nathan and Mauz, 2008) where we described, calculated and modeled the impact of carbonate on the dose rate. Since then the software (called '*Carb*') has been employed in several studies (Mauz et al., 2009, 2012, 2013) resulting in a clear and unequivocal impact on the accuracy of the OSL ages which allowed to improve sedimentological models on the 100 ka Milankovitch time scale (Mauz et al., 2013). This increased the confidence that the dose-rate model is a reliable tool to correct for post-depositional chemical alterations involving carbonate.

Since publication, Nathan and Mauz, 2008 received some attention, but it failed to incentivise dose-rate modeling where it was - according to sample description in the relevant publications - certainly appropriate. We conclude that more attention needs to be drawn to this issue by (i) providing a clear and comprehensive description of the impact of carbonate on the dose rate and by (ii) making the code available to users.

When Nathan and Mauz (2008) was published, *Carb* suffered from two weaknesses: (1) correction of U-series secular disequilibrium caused by post-mortem U-uptake of mollusk shells was not possible and (2) interstitial carbonate was assumed to be inert while no data were available to (dis-)prove this.

With this short paper we wish to encourage users to appreciate (i) the importance of dose-deposition efficiency and its dependence on material properties and (ii) the significance of dose-rate change over time. We aim at removing doubts and misunderstandings about the impact of carbonate on dose rate, at explaining the code including its update, its assumptions and limitations and at providing instructions on how to use it.

For description of the underlying physics, in particular the infinite matrix concept, calculation of attenuation factors, determination of mass stopping powers and mass absorption coefficients, the reader

is referred to the original paper (Nathan and Mauz, 2008), to Guérin et al. (2012), Guérin and Mercier (2012) and, of course, to Aitken (1985) and references herein.

## Carbonate and the cementation process

Cementation is the process which turns loose sediment into rock. It occurs in marine, lacustrine, fluvial and aeolian environments through new minerals (forming cements) being precipitated as a matrix in the pores between the primary sediment particles (i.e. detrital components). A cemented sediment is then composed of primary components (e.g., detrital quartz, feldspar, limestone particles), matrix (i.e. cement) and "empty" pore space (filled by water or air). Cement formation is caused by precipitation of calcium carbonate (CaCO<sub>3</sub>) minerals from a pore fluid that is oversaturated with respect to a carbonate phase. The process of cementation and its timing depends largely on the pH and temperature of the water-sediment mixture, the availability of CO<sub>2</sub> from bacterial oxidation, permeability of the sediment and hydrodynamic conditions. The process of cementation can start during sedimentation (syn-sedimentary) or after sedimentation (burial). During burial dissolution, reprecipitation and recrystallisation of the carbonate mass can occur. These processes follow the relative thermodynamic stability of the carbonate minerals (e.g., calcite, aragonite) and the chemistry of the pore fluid with the end-point of the process being chemical stability.

## The dose-rate correction factor

At the time of sedimentation of the detrital components the pore material is air and water. At  $t=0$  which is the time when the pore material starts changing, carbonate precipitates in the existing pore space where it gradually replaces water or air. At  $t=1$  the change ceased and the carbonate content is achieved as measured today (for details of this concept see Nathan and Mauz's Fig 3). When the

material of the pore space changes, so do the energy spectra of beta and gamma rays and the related energy absorption.

The relative energy absorption of the pore material (i.e. water, air, carbonate) compared to the primary sediment components is expressed by the correction factor  $x$  and was computed by Zimmerman (1971) as the effective ratio of mass stopping powers of water and aluminium for beta radiation and the effective ratio of mass absorption coefficients for gamma radiation. With  $x=1$  detrital sediment components and pore material (matrix) absorb the same average amount of dose over a given radiation spectrum. Table 1 lists the correction factors in terms of the different ratios (carbonate/sediment and water/sediment) for beta radiation. The values demonstrate an increase of the dose to quartz deposition when water is replaced by carbonate (because "water absorbs more than its fair share"; Aitken, 1985, p. 69). They also show that the transition from water to carbonate becomes significant for the dose rate when the carbonate content exceeds around 20% of the total pore material.

	$m_c/m_s$			
$m_w/m_s$	<b>0</b>	<b>0.04</b>	<b>0.20</b>	<b>1.00</b>
<b>0</b>	-	0.99	0.99	0.99
<b>0.04</b>	1.19	1.09	1.03	<i>1.00</i>
<b>0.20</b>	1.20	1.09	1.09	<i>1.02</i>
<b>1.00</b>	1.19	<i>1.18</i>	<i>1.15</i>	<i>1.09</i>

**Table 1.** The correction factor  $x$  for beta radiation for water and carbonate to sediment mass ratios ( $m_s$  = sediment mass;  $m_c$ =carbonate mass;  $m_w$  = water mass). Values in italic are theoretical because they do not exist in nature. For details regarding radioactive elements see Nathan and Mauz (2008).

For beta radiation Zimmerman (1971) calculated  $x=1.25$  for water. Our value is 1.19 in agreement with Guérin and Mercier (2012). The values of  $x$  decrease by up to 17% (i.e. from 1.19 to 0.99) when all water is replaced by carbonate. For gamma radiation the difference is around 11% when  $x=1.14$  (Zimmerman, 1971) is used for water. Aitken and Xie (1990) computed  $x=1.065$  and our analysis revealed 1.06-0.98 for K, Th and U in water using the same data as Aitken and Xie (1990) but excluding secondary electrons. But because secondary electrons play a role in gamma dose-rate absorption and because Guérin and Mercier (2012) found values between 1.19 and 1.13 using the Monte Carlo simulation software GEANT4, the original Zimmerman value is

still valid. Guérin and Mercier (2012) also show that for the energies considered (0.05-3 MeV) the  $x$  values increase with decreasing particle size with a trend towards a limiting value of 1.20 for particle sizes between 20-500  $\mu\text{m}$ .

### The activity of carbonate

Most sedimentary environments are a sink for radionuclides originating from detrital input. In addition to detrital Uranium there is soluble Uranium occurring in two oxidation states ( $\text{U}^{4+}$  and  $\text{U}^{6+}$ ), but in most environments the soluble  $\text{U}^{6+}$  form dominates. Thorium mainly occurs in the 4+ oxidation state and is largely insoluble in natural waters. Groundwaters, rivers or seawater therefore contain considerable amounts of dissolved U but virtually no Th. In rocks of geological age  $^{238}\text{U}$  is in activity equilibrium with its daughter nuclides including  $^{234}\text{U}$ . However, the  $\alpha$ -recoil effect on the  $\alpha$  decay leads to preferential leaching of  $^{234}\text{U}$  and hence fractionation between  $^{234}\text{U}$  and  $^{238}\text{U}$  in the leachate. Thus,  $^{234}\text{U}/^{238}\text{U}$  isotope ratios of ground- and river-waters are usually higher than the equilibrium value. The modern  $^{234}\text{U}/^{238}\text{U}$  activity ratio in marine waters is around 1.146 (Chen et al., 1986; Robinson et al., 2004).

Pore waters provide means for U transport into and out of the sediment. There are various possible scenarios such as U exchange between dissolved and particulate phase, U uptake, U loss or U mobilisation and any organic material being in exchange with the pore waters is affected by these processes. U uptake is known to be a dominant feature for organic carbonate such as mollusc shells. But sediment cement is a result of an inorganic precipitation process and thus, little can be inferred from shells about U uptake processes occurring in interstitial carbonate. The few available data, generated by us (for technical details see Appendix), are displayed in Figs 1 and 2. Fig. 1 shows concentrations of 0 ppm up to around 5 ppm in carbonate cement. In Fig. 2 the U uptake in shell and carbonate matrix is plotted against the age of the sample. It shows that with time the uptake in shell can increase (not in all samples) while there is no increase of U concentration in the matrix. This suggests that, if uptake takes place, it happens during primary cementation and not later during burial. The assumption of an inert carbonate matrix (Nathan and Mauz, 2008) is therefore contested.

We conclude from these data that gradually growing carbonate cement can contribute from nil up to several percent to the dose rate. How this gradual increase ultimately impacts on the dose rate over time depends largely on the ratio between changing U content on the one side and constant Th and K content on the other side. The more other radioactive

sources (K, Th) are part of the detrital sediment component in a sediment, the smaller will be the relative difference between onset and final dose rate (where onset dose rate represents the radiation field at the time of deposition and the final dose rate is the one of chemical stability).

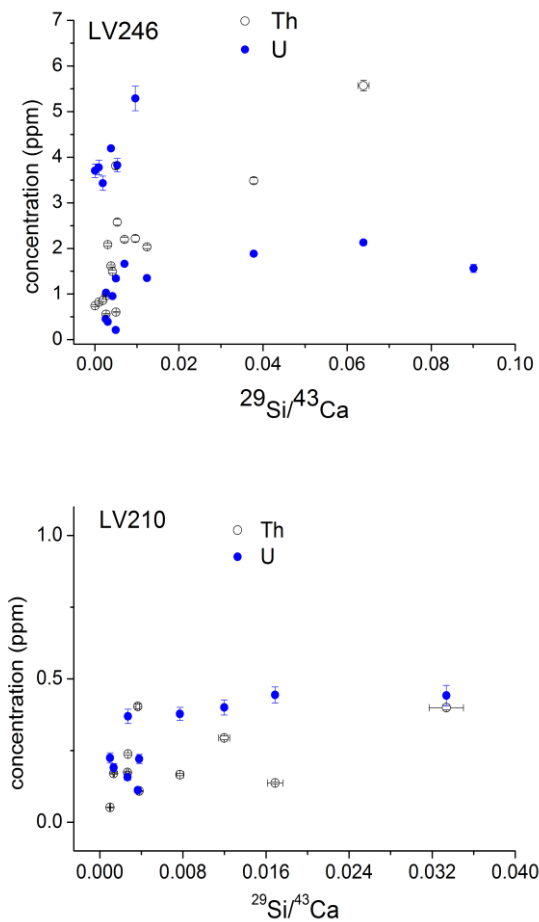


**Figure 1:** The concentration of U and Th in carbonate cement plotted against Si/Ca for two samples originating from different geological regions. Data with Si/Ca  $\sim$  0.00 can be used for interpreting the activity of the carbonate component in the sample. LV246 originate from an around 6 ka old aeolian deposit on the south Adriatic coast (Italy) where the bedrock is limestone. LV210 originate from an around 57 ka old aeolian deposit on the Levant coast (Israel) where the bedrock is limestone. These data indicate a large variability of activity (0.1-5.5 ppm) of the secondary carbonate.

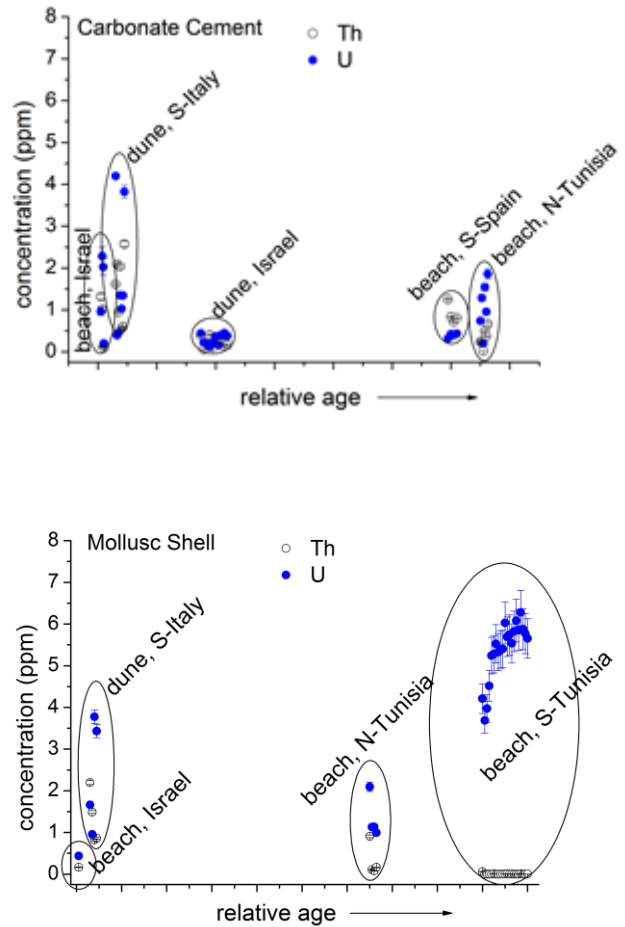


**Figure 2:** The concentration of U and Th in mollusc shells and carbonate cement plotted against relative age of samples. The data suggest early uptake of U in secondary carbonate whereas the uptake in mollusc shells can be continuous in time. In two samples (S-Italian dune sediment and N-Tunisian beach sediment) the U-uptake is similar in amount; in one sample (Israel beach sediment) more U is up-taken in the cement than in shells. For measurement details see Appendix.

The accurate estimation of a changing dose rate over time requires knowledge on the initial U activity ratio. In a closed system this ratio is constant and there is compelling evidence that virtually no natural carbonate environment behaves as a closed system (e.g., Thompson et al., 2003; Edwards et al., 2009). We measured shell fragments and carbonate matrix in two samples (LV111 and LV107) for their  $^{230}\text{Th}/^{238}\text{U}$  and  $^{234}\text{U}/^{238}\text{U}$  ratios (for technical details see Appendix). The  $^{230}\text{Th}/^{238}\text{U}$  ratio allowed calculating an apparent age from which the apparent initial  $^{234}\text{U}/^{238}\text{U}$  can be deduced (Fig. 3). For LV111, both

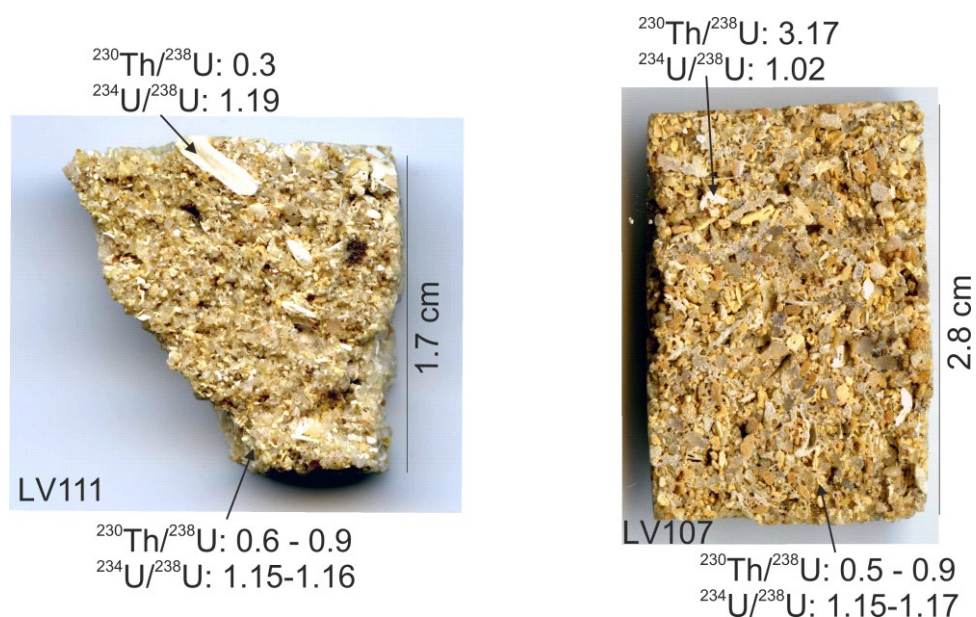


**Figure 3:** The activity ratios in samples LV111 and LV107. For data see Table 2. The upper arrows in each photo indicate the shell, the lower arrows the cement matrix.

shell and carbonate matrix have mean measured  $^{234}\text{U}/^{238}\text{U}$  activities that are greater than the marine value of 1.146. But with the large uncertainty associated with laser ablation  $^{234}\text{U}/^{238}\text{U}$  isotope ratio measurements, the measured ratios for matrix actually overlap with the marine value. The shell of

LV111 has a measured  $^{234}\text{U}/^{238}\text{U}$  activity of 1.19 and an apparent initial  $^{234}\text{U}/^{238}\text{U}$  activity of 1.21 indicating an open system. Assuming an initial marine signature for the matrix, the measured

ID	$^{230}\text{Th}/^{238}\text{U}$	$\pm$	$^{234}\text{U}/^{238}\text{U}$	$\pm$	Age (ka)	$\pm$	Initial $^{234}\text{U}/^{238}\text{U}$	$\pm$
LV111-shell	0.3030	0.010	1.1915	0.010	31.8	1.19	1.210	0.011
LV111-matrix1	0.9093	0.043	1.1641	0.019	156.0	16.69	1.255	0.027
LV111-matrix2	0.5612	0.030	1.1589	0.024	71.0	5.68	1.194	0.028
LV107-matrix1	0.5415	0.059	1.1452	0.036	68.8	10.84	1.176	0.043
LV107-matrix2	0.8896	0.051	1.1704	0.022	147.2	18.19	1.258	0.031
LV107-shell	3.1654	0.095	1.0248	0.023	-	-	-	-

**Table 2:** The activity ratios in samples LV111 and LV107 and their related uncertainties. Analytical errors are at 95 % confidence level. Age (ka) refers to the apparent U/Th age of the relevant material measured and does not represent the depositional age of the sample. For calculation of those values the reader is referred to the Appendix.

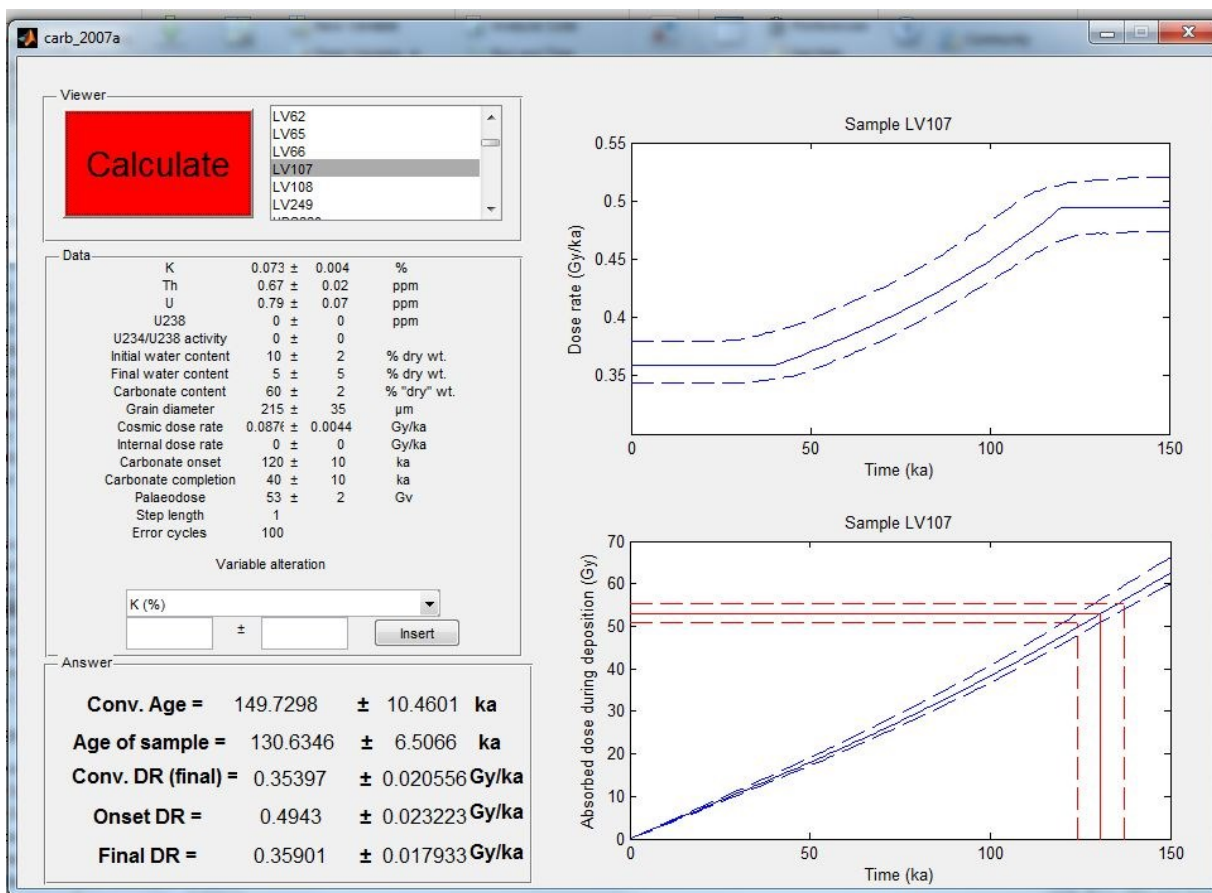


**Figure 4:** The upper graph shows the dose rate over time (solid blue line) with 95% confidence interval (dashed blue line). The water content is reduced proportionately to the accumulation of carbonate in the sediment pores until it reaches a new constant level. The lower graph shows the increase in absorbed dose over time (blue solid line) with 95% confidence interval (dashed blue line) as a function of the integrated dose rate. The age of the sample is estimated by projecting the  $D_e$  (red line) and the error onto the dose function.

$^{234}\text{U}/^{238}\text{U}$  activity ratios of 1.159 and 1.164 and the apparent initial  $^{234}\text{U}/^{238}\text{U}$  activity ratios of 1.19 and 1.26 also indicate an open system for the matrix. The shell of LV107 has a measured  $^{234}\text{U}/^{238}\text{U}$  activity of 1.02. Here, the measured  $^{230}\text{Th}/^{238}\text{U}$  activity ratio of 3.17 is in excess of natural activity ratios and suggests U loss for this sample, probably after initial U uptake into the shell. No initial  $^{234}\text{U}/^{238}\text{U}$  ratio can be calculated for this shell. The matrix has measured  $^{234}\text{U}/^{238}\text{U}$  activity ratios of 1.145 and 1.17 and the apparent initial  $^{234}\text{U}/^{238}\text{U}$  activity ratios of 1.176 and 1.258 also indicate an open system for this matrix (for data see Table 2 and Fig. 3).

These data confirm the open system behaviour of samples that contain inorganic (cement) and organic (shell) carbonate. To date, the impact of the activity ratio on the dose rate is unknown.

#### Description of the code

*Carb* accounts for the post-depositional chemical alteration of the sediment caused by cementation and for post-mortem Uranium uptake in mollusk shells. The dose rate over time is constructed as a series of values (Fig. 4) where the water content is reduced proportionately to the accumulation of carbonate in the sediment pores until it reaches a new constant level. The age of the sample is estimated as the length of time needed for the integrated dose rate to equal the equivalent dose ( $D_e$ ). Uncertainties in the dose rate and ages are estimated using a Monte-Carlo approach.

*Carb* is written for the MATLAB software. The MATLAB script is called *Carb.m* and the input file is *SAMPLE\_DATA.txt*. The script contains all necessary steps to build the dose-rate model based on the data provided in the input file.

After loading the two files into the workspace of MATLAB and running the script, the command surface appears (Fig. 4). Here, the user selects the sample. The input values of the selected sample appear below the calculate button. These can be modified using the 'Variable Alternation' option by selecting the variable, type the new value, click insert and then calculate. The script provides 5 answers: (1) the conventional age based on the conventional dose rate, (2) the conventional dose rate, (3) the age of the sample as modelled by *Carb*, (4) the dose rate before secondary carbonate started forming (onset) and (5) the final dose rate (Fig. 4). The final dose rate and the conventional dose rate must agree within 1.5%.

### Data and data input

Data required are: K, Th, U,  $^{238}\text{U}$ ,  $^{234}\text{U}/^{238}\text{U}$ , water content initial and final, carbonate content, grain diameter, cosmic dose rate, internal dose rate, onset and termination of carbonate formation, De, step size, error cycle (i.e. the number of Monte Carlo iterations). For units of the input data see Fig. 4. Most of these data are required for conventional dose-rate estimation and the reader is referred to Aitken (1985) for details.  $^{238}\text{U}$  is the initial detrital U before secondary carbonate started forming.  $^{238}\text{U}$  and the U-activity ratio is ideally determined by relevant techniques (e.g. ICP-MS) or taken from literature (Chen et al., 1986; Gascoyne, 1992) or inferred from the U/Th ratio (see Ivanovich and Harmon, 1992 for the U/Th ratio in the upper earth crust).

Data input is managed through the file SAMPLE\_DATA.txt. The input file has the format

LV111	LV107
0.105	0.073
0.004	0.004
0.650	0.670
0.002	0.020
1.250	0.790
0.080	0.070

where each column represents the data of one sample and the values of each row are followed in the subsequent row by their respective error values. For order of data see also Fig. 4.

### Underlying assumptions of the code

The code is based on the following assumptions which are be discussed below: (1) the carbonate content is secondary carbonate resulting from the cementation process; (2) the growth of carbonate cement is linear and it is inversely correlated with the moisture content; (3) water and carbonate are inert and therefore the number of decays within a unit volume is constant; (4) U uptake by biological

remains and initial U-activity ratio is known; (5) there is no migration of radioisotopes within the sediment; (6) the sediment is homogeneous at any particular time and (7) the ionising radiation is in charged particle equilibrium.

Assumption (2) is relatively robust because the deviation from linearity is small over time. Assuming constant number of decays per unit volume of sediment (ass. 3) and absence of radioisotope migration (besides U-uptake; ass. 5) is more problematic. The series of constructed values as shown in Fig. 4 is in nature more variable between the onset and termination of dose-rate change. Also, the equilibrium of the charged-particle fluence is only an approximation for sedimentary environments because spatial variation of the fluence is a function of particle size and pore-size distribution as well as lithic and pore-size structures (e.g., Guérin et al., 2012).

### Discussion

The purpose of this section is to discuss and highlight important aspects and questions of dose-rate modelling for carbonate rich samples.

*The timing of cementation during burial:* Petrographic analyses allow distinguishing between early and late cementation and thereby approximating the timing of onset and termination. In addition, *Carb* allows testing different scenarios. Moreover, Nathan and Mauz (2008) showed that *Carb* is relatively insensitive to the timing of the carbonate ingrowth. In other words, the lack of the ability to quantify onset and termination of cementation has a minor impact on the accuracy of the model output.

*Instantaneous cementation:* If the cement formation is instantaneous, the change of dose rate over time may indeed be negligible. However, instantaneous cementation is very rare in nature (Morse and Mackenzie, 1990) and the assumption would require evidence through petrographic analysis.

*The change of dose rate over time in cemented sediments:* Secondary carbonate, which has energy absorption coefficients that differ from air or water, precipitates in the pore space over time and not at once. The exact time span is hard to determine because sediment carbonate geochemistry is a function of thermodynamics, dissolution and precipitation kinetics and surface chemistry of carbonate minerals. From a conceptional point of view we can say that for any given late Quaternary sediment it may take  $10^2$ - $10^5$  years to reach chemical stability. While the  $10^2$  years timescale is well known in carbonate sedimentology (e.g. Morse and Mackenzie, 1990) because it is an interesting

exception in nature, the  $10^5$  years timescale is used here by the author to illustrate that chemical stability may not be reached over the time span covered by the dosimeter.

*Does the carbonate content impact on the dispersion of  $D_e$  values?* The answer to this question requires comparison of the radioactivities of matrix (carbonate) and primary detrital components where the latter potentially hosts a radioactive hotspot. Likewise, it requires simulation work. In the absence of this work a brief estimation can be made: The range of 1 MeV electrons is in water twice as large as it is in carbonates. As a result, radiation from hotspots would reach a smaller volume of detrital components when carbonate covers the pore space instead of water or air. Taking the results of Mayya et al. (2006) into account, it is likely that the dispersion of  $D_e$  values increase with increasing carbonate content.

*Daylight bleaching and carbonate ingrowth:* The deposition of the dosimeter as part of the detrital component of the sediment occurs prior to cementation and there are several orders of magnitude time difference between bleaching and (instantaneous) cementation.

*Detrital versus secondary carbonate:* The differentiation and quantification of detrital versus secondary carbonate requires petrographic analysis. If the detrital component is dominant, i.e. if the sample is barely cemented, the change of dose rate over time is negligible. Detrital carbonate originating from limestone bedrock is mostly inert and contributes to the heterogeneity of the beta radiation field in the sample. Typically, the size of the limestone particles is different from that of the other primary sediment components due to different material properties. In this case the carbonate element creates a geometry issue of the infinite matrix concept, which is discussed by Guérin et al. (2012).

*Secondary carbonate and water:* Based on fundamental principles and empirical evidence in sedimentology, it is expected that the texture of the sediment (e.g. packing of components) does not change during the cementation process and *Carb* therefore assumes that the carbonate cement is inversely correlated with the moisture content. Thus, during burial the total volume of the sediment remains approximately the same, while density and mass change.

*By how much does the dose rate change due to secondary carbonate?* If, for example, 40% carbonate matrix was precipitated syn-sedimentarily,

the change of dose rate over time would be negligible. The correction factor would be different but this difference would be small. It is the interplay between all parameters that affects the accuracy of the age estimate and this cannot be assessed by examining parameters individually.

*Does the ingrowth of secondary carbonate result in age underestimation?* The carbonate infill has different dose-deposition efficiencies, which can result in both under- and overestimation of age if this efficiency is not taken into account. Nathan and Mauz (2008) and Mauz et al. (2009) show however, that dose-rate modelling using *Carb* results in lower ages compared to a steady state dose-rate estimation. The lower ages are a consequence of the lower dose-deposition efficiency of carbonate compared to water under the assumption that the carbonate matrix is inert. But even if the carbonate matrix is not inert, the data plotted in Figs 1, 2 and 3 suggest that a decrease of dose rate during burial is more likely than an increase. The rationale here is that the data (Fig. 2) indicate an early uptake of U in the carbonate matrix while the absorption of radiation through carbonate is continuous throughout the time of burial and more effective than through water. When plotting dose rate against burial time (Fig. 4), the slope of the curve would probably be less steep for a sample with an active carbonate matrix compared to a sample with an inert matrix.

*Field appearance of cemented sediment deposits:* Well-preserved beds of a cemented sediment deposit are those with a spatially relatively constant cement to porosity ratio and are therefore the preferred sampling target.

*Carb and petrographic analyses:* Although beneficial, *Carb* does not require petrographic analyses. It requires quantification of the carbonate content, which is a straightforward laboratory analysis.

*Carbonate ingrowth and the contribution of U to the dose rate:* In general, the contribution of U to the effective dose rate is small if the sample is from a closed sedimentary system. While U can create secular disequilibrium in the sediment, for cemented samples it is the energy absorption efficiencies of different materials for beta and gamma radiation originating from K, Th and U that are important.

*Can the modern marine U activity ratio be adopted for all cemented samples?* In theory not, because the carbonate cement could have precipitated from meteoric water with a very different initial activity ratio. In practice, the impact of an inaccurate activity

ratio on the dose rate is probably small unless U is the only radioactive source in the sediment.

### Final remarks

In most carbonate-rich samples the dose rate generated by external alpha, beta and gamma radiation is low (e.g. <1 Gy/ka) to very low (e.g. 0.3 Gy/ka). A low external dose rate raises the importance of the internal (i.e. within the dosimeter) and the cosmic dose rate.

The application of the model does not require detailed understanding of the underlying physics, carbonate geochemistry or MATLAB software.

The robustness of the algorithm is limited. Extreme sample values cannot be handled. Thus, the sample must conform to the carbonate dose-rate model and its assumptions as described above. Adjusting parameters is an advantage of the code, but this option is probably restricted to users with expert knowledge.

The script file, a template file for the data input and further instructions can be downloaded from the Ancient TL webpage.

### Acknowledgements

We are grateful for the input of the two reviewers Guillaume Guerin and Ashok Singhvi. We also thank the editor for her thoughtful comments.

### References

- Aitken, M.J., 1985. Thermoluminescence Dating. Academic Press, London, 378pp.
- Aitken, M.J., Xie, J., 1990. Moisture correction for annual gamma dose. *Ancient TL* 8, 6–9.
- Chen, J.H., Edwards, R.L. and Wasserburg, G.J., 1986.  $^{238}\text{U}$ - $^{234}\text{U}$ - $^{232}\text{Th}$  in seawater. *Earth and Planetary Science Letters*, 80, 241-251.
- Edwards, R.L., Gallup, C.D. and Cheng, H. Uranium-series dating of marine and lacustrine carbonates. In: Bourdon, B., Henderson, G.M., Lundstrom, C.C. and Turner, S.P. (eds), *Uranium-series geochemistry. Reviews in Mineralogy & Geochemistry* 52, 363-405pp.
- Gascoyne, M., 1992. Geochemistry of the actinides and their daughters. In: Ivanovich, M., Harmon, R.S. (Eds.), *Uranium-series Disequilibrium: Applications to Earth, Marine, and Environmental Sciences*, pp. 34-61.
- Guérin, G., Mercier, N., Nathan, R., Adamiec, G. and Lafrays, Y., 2012. On the use of the infinite matrix assumption and associated concepts: A critical review. *Radiation Measurements* 47, 778-785.
- Guérin, G. and Mercier, N., 2012. Preliminary insight into dose deposition processes in sedimentary

- media on a scale of single grains: Monte Carlo modelling of the effect of water on the gamma dose rate. *Radiation Measurements* 47, 541-547.
- Hoffman, D.L., Spötl, C. and Mangini, A., 2009. Micromill an in situ laser ablation sampling techniques for high spatial resolution MC-ICPMS U-Th dating of carbonates. *Chemical Geology* 259, 253-261.
- Ivanovich, M., Harmon, R.S., 1992. Uranium-series disequilibrium: Applications to Earth, Marine, and Environmental Sciences.
- Mauz, B., Fanelli, F., Elmejdoub, N., Barbieri, R., 2012. Coastal response to climate change: Mediterranean shorelines during the last interglacial (MIS 5). *Quaternary Science Reviews* 54, 89–98.
- Mauz, B., Hijma, M.P., Amorosi, A., Porat, N., Galili, E., Bloemendal, J., 2013. Aeolian beach ridges and their significance for climate and sea level: concept and insight from the Levant coast (East Mediterranean). *Earth Science Reviews* 121, 31–54.
- Mauz, B., Elmejdoub, N., Nathan, R.P. and Jedoui, Y., 2009. Last interglacial coastal environments in the Mediterranean–Saharan transition zone. *Palaeogeography, Palaeoclimatology, Palaeoecology* 279, 137–146.
- Mayya, Y.S., Morthekai, P., Murari, M.K. and Singhvi, A.K., 2006. Towards quantifying beta microdosimetric effects in single-grain quartz dose distribution. *Radiation Measurements* 41, 1032-1039.
- Nathan, R.P. and Mauz, B., 2008. On the dose-rate estimate of carbonate-rich sediments for trapped charge dating. *Radiation Measurements* 43, 14-25.
- Morse, J.W. and Mackenzie, F.T., 1990. Geochemistry of sedimentary carbonates. *Developments in Sedimentology* 48. Elsevier, 707p.
- Robinson, L.F., Belshaw, N. and Henderson, G.M., 2004. U and Th concentrations and isotope ratios in modern carbonates and waters from the Bahamas. *Geochimica et Cosmochimica Acta*, 68, 1777-1789.
- Thompson, W.G., Spiegelmann, M.W., Goldstein, S.L., Speed, R.C., 2003. An open-system model for U-series age determinations of fossil corals. *Earth and Planetary Science Letters* 210, 365–381.
- Zimmerman, D.W., 1971. Thermoluminescence dating using fine grains from pottery. *Archaeometry* 13, 29–52.

### Reviewer

G. Guerin, A. Singhvi

## Appendix

### *Measuring the Uranium and Thorium element concentrations (Figures 1 and 2):*

Aa New Wave UP193HE laser coupled to a Thermo Element 2 sector field ICPMS was used. The laser was operated at a repetition rate of 5 Hz, a spot diameter of 30  $\mu\text{m}$  and an energy density of 4-5  $\text{J}/\text{cm}^2$ . The counting time for a single analysis was 120 s with 60 s measuring gas blank to establish the background count rates and 60 s for laser ablation. The following isotopes were used for elemental analysis:  $^{29}\text{Si}$ ,  $^{43}\text{Ca}$ ,  $^{44}\text{Ca}$ ,  $^{232}\text{Th}$  and  $^{238}\text{U}$ . Total dwelling time on each peak was 60 ms. The NIST 610 glass standard was used for calibrating the relative element sensitivities. The concentrations were taken from Pearce et al. (1997). The CaO concentration of the carbonate samples was assumed to be 55 wt %. With a laser penetration depth of 30-50  $\mu\text{m}$  and a laser spot size of 30  $\mu\text{m}^2$ , the purity of the spot in terms of "carbonate only" was ascertained by plotting the data of each spot against their Si/Ca ratio (Figs 1 and 2) where Si/Ca  $\sim 0$  indicates pure carbonate.

### *Measuring the activity of inorganic (pore material) and organic (shell) carbonate (Figure 3):*

The samples were analysed using laser ablation (LA) multi-collector (MC) - inductively coupled mass spectrometry (ICPMS) U-Th disequilibrium techniques following the method outlined by Hoffmann et al. (2009). All MC-ICPMS measurements were performed using a ThermoFinnigan Neptune coupled with a New Wave Research UP193HE ArF Excimer laser system. Samples were placed in a laser sample cell together with an in-house carbonate U-Th LA calibration sample, which is a secular equilibrium calcite 'standard' for correction of instrumental biases of LA U-Th isotope measurements on  $\text{CaCO}_3$ . Ablation is done using He as carrier gas which is mixed with Ar sample gas and  $\text{N}_2$  in a quartz mixing cell before injection into the Ar plasma. Typical laser power density is 5  $\text{J}/\text{cm}^2$  at 70 % power output, for U-Th isotope LA measurements presented in this study we used 7 Hz repetition rate and a 90  $\mu\text{m}$  diameter spot size. A LA measurement was done on a 0.5 mm long track, ablated by moving the laser spot at a speed of 20  $\mu\text{m}/\text{s}$  along the track in 6 passes. A standard - sample - standard bracketing procedure was applied and data collection and corrections were carried out following Hoffmann et al. (2009).

### *Calculation of age and apparent initial $^{234}\text{U}/^{238}\text{U}$ ratios (Table 2):*

$^{230}\text{Th}/^{238}\text{U}$  and  $^{234}\text{U}/^{238}\text{U}$  at the present time  $t$  were measured. The following equation is used to (iteratively) calculate the age  $t$ :

$$\left(\frac{^{230}\text{Th}}{^{238}\text{U}}\right)(t) = (1 - e^{-\lambda_{230} t}) + \left(\left(\frac{^{234}\text{U}}{^{238}\text{U}}\right)(t) - 1\right) \frac{\lambda_{230}}{\lambda_{230} - \lambda_{234}} (1 - e^{-(\lambda_{230} - \lambda_{234}) t})$$

Decay constants  $\lambda$  are  $9.1577 \times 10^{-6} \text{ a}^{-1}$  for  $^{230}\text{Th}$ ,  $2.826 \times 10^{-6} \text{ a}^{-1}$  for  $^{234}\text{U}$ ,  $1.55125 \times 10^{-10} \text{ a}^{-1}$  for  $^{238}\text{U}$ . Using the calculated age  $t$ , the apparent initial ratio  $^{234}\text{U}/^{238}\text{U}$  follows from

$$\left(\frac{^{234}\text{U}}{^{238}\text{U}}\right)(t) = \left(\left(\frac{^{234}\text{U}}{^{238}\text{U}}\right)_{\text{init.}} - 1\right) e^{-\lambda_{234} t} + 1$$

## Thesis Abstracts

---

**Author:** Alessia Artesani  
**Thesis Title:** Surface dating of bricks, an application of luminescence techniques  
**Grade:** Masters  
**Date:** April 2014  
**Supervisors:** M. Martini, A. Galli  
**Address:** Dipartimento di Scienza dei Materiali, Università degli Studi di Milano-Bicocca, Milano (Italy)

Luminescence techniques are nowadays a powerful tool to date archaeological ceramic materials and geological sediments. In particular thermoluminescence (TL) is widely used for brick dating, to reconstruct the building chronology of urban complexes. However, it can be sometimes inconclusive, since TL assesses the firing period of bricks that can be reused in different structures, even several centuries later. This problem can be circumvented by using a dating technique which uses a resetting event different from the last heating of the material: an ideal candidate is OSL, exploiting the last exposure to sunlight of the brick surface, which resets the light sensitive electron traps until the surface is definitely shielded by mortar and superimposed bricks. This advanced application of the OSL technique (surface dating) has been successfully attempted on rocks, marble and stone artifacts, but not routinely on bricks.

A recent conservation campaign at the Certosa di Pavia complex (Italy) gave the opportunity to sample some bricks belonging to a XVII century collapsed wall, still tied to their mortars. This thesis work aimed at testing the surface dating technique, by having the opportunity to compare the dating results with precise historical data. The study was carried out in two steps; in the first part the material behaviour after sunlight exposure has been checked. A non-rapid decrease of surface signal as consequence of a brief exposure to light, results in a limit the applicability of surface dating technique. In the case of samples examined here, a reduction of the luminescent signal by 75 % was found after 6 hours of exposure to sunlight, and a decrease of 90 % after 60 days of exposure. The response times of the material are in agreement with those reported in the literature for other types of materials.

The dependence of OSL/IRSL signal on the penetration depth of sunlight, on the exposure time and temperature has been studied. Freshly exposed

surfaces, cut in the laboratory at the middle of bricks, were exposed to sunlight for different periods (from 60s to 2 months), and the external 0.5 mm layer appeared to be fully bleached after a few hours of exposure. The bleaching of the deeper layer needed at least 1 month of exposure.

Five bricks were dated applying both TL (MAAD technique) and OSL (SAR protocol) on bulk and surface portion of the samples. The results showed that the bulk OSL EDs well matched the TL EDs. They were however systematically and significantly higher than the surface ones, shielded by the mortar layers. This was a strong evidence of the reuse of the material: the bulk date (XI century) is associated to firing in kiln, while the surface date (1530-1650 AD) was in agreement with the known age of the wall.

**Author:** Trine Holm Freiesleben  
**Thesis Title:** Developing a Method for Luminescence Dating of Rock surfaces  
**Grade:** Masters  
**Date:** September 2014  
**Supervisors:** Søren Hvidt, Bo Jakobsen, Andrew Murray, Reza Sohbati  
**Address:** Roskilde University & The Nordic Centre for Luminescence Research

Interest in the optical luminescence dating (OSL) of rock surfaces has increased significantly over the last few years, as the potential of the method has been realised. In this study we investigate the information available in blue-stimulated luminescence depth profiles into the surfaces of 4 quartz-rich cobbles from a Neanderthal site (Les Roches d'Abilly) in western France, and IR stimulated luminescence depth profile from a feldspar-rich granite whetstone from an Iron Age villages near Aarhus in Denmark.

These profiles show qualitative evidence for multiple daylight exposure and burial events. To quantify both burial and daylight exposure events a new model is developed. The existing model describing the evolution of luminescence depth profiles is expanded to include burial before and after light exposure, and the possibility of repeated sequential daylight exposure and burial events. By determining the burial ages from the surface layers of the cobbles and by investigating the fitted luminescence profile, it is concluded that all cobbles were apparently well

bleached before burial. This indicates that the estimated burial ages are reliable. In all cases the burial age of the most recent burial event is consistent with the expected age (quartz OSL on sediments from Les Roches d'Abilly and archaeological context for the Aarhus site). In addition, a recent known daylight exposure event provides an approximate calibration for daylight exposure events.

This study thus confirms the suggestion that rock surfaces contain a record of daylight and burial history. Rock surfaces can therefore be dated with confidence, and it may be possible to determine a daylight exposure history using a known natural light exposure as calibration. Besides developing and applying the mathematical model, a preparation method for the samples used in this study has been developed. This development was based on knowledge of the chemical structure and properties of quartz and feldspar, together with X-ray fluorescence (XRF) measurements of full rock slices before and after chemical treatment.

It is concluded that, in order to extract pure quartz grains from the French samples, hydrogen chloride (HCl) should be added before etching with hydrofluoric acid (HF). If HCl is not used first to remove calcium carbonate from the rock slices, HF cannot attack and remove feldspar grains. It is also shown that the absence of feldspar in XRF analysis does not necessarily indicate that there is no infrared luminescence sensitivity, indicating that feldspar has not been completely removed.

**Author:** Marine Frouin  
**Thesis Title:** Feldspars as support for the luminescence dating of archaeological deposits and quaternary sequences of Aquitaine  
**Grade:** Ph.D.  
**Date:** December 2014  
**Supervisors:** Norbert Mercier and Christelle Lahaye  
**Address:** Université de Bordeaux Montaigne, Esplanade des Antilles, 33607 Pessac cedex, France

Currently available chronological information for Middle Palaeolithic sites in southwestern France precludes the establishment of a robust chronological framework. For these early periods, developing such a framework relies upon important methodological advancements in numerical dating techniques.

The results of this study are essentially based on OSL dating of sedimentary feldspars and quartz. Focusing on the most commonly employed luminescence signals (IRSL, pIR-IRSL), it was possible to more clearly evaluate the reliability of dates obtained on K-feldspars. A dating protocol for these materials based on their radioluminescence signal (IR-RF) was also developed.

Optical luminescence dates were produced for six major archaeological sites: (Marillac, Charente), Combe Brune 2 (Creysse, Dordogne), Roc de Marsal (Campagne, Dordogne), Artenac (Saint-Mary, Charente), La Quina (Gardes-le-Pontaroux, Charente) et La Ferrassie (Savignac-de-Miremont, Dordogne). Collating the results for each archaeological level allowed the coherence of the dates to be tested and a reliable chronological sequence to be proposed for each site.

The different human occupations, characterised by their industrial attribution, could be placed within a chronological framework that incorporates regional palaeoenvironmental and palaeoclimatic variations. Finally, several observations provide new insights for our understanding of Neanderthal cultures.

**Keywords:** *Middle Palaeolithic, chronological framework, potassic feldspars, quartz, optical luminescence, radioluminescence, palaeoclimate, palaeoenvironment, Neanderthal cultures.*

**Author:** Xiao Fu  
**Thesis Title:** Development of luminescence dating using feldspar and its application to river terraces in north piedmont of Chinese Tian Shan  
**Grade:** Ph.D.  
**Date:** October 2014  
**Supervisor:** Sheng-Hua Li  
**Address:** Department of Earth Sciences, the University of Hong Kong, Hong Kong, China

This thesis study focused on developing luminescence dating procedures for feldspar, and applying the luminescence dating technique to fluvial terraces of Anjihai River in the northern piedmont of Tian Shan range, China, to evaluate the deformation rate of the Anjihai anticline in the late Quaternary.

In development of luminescence dating methods, a low temperature multi-elevated-temperature post-infrared stimulated luminescence (MET-pIRIR) protocol has been proposed for measuring the Holocene samples using K-feldspar. Progressively

increasing IR stimulation temperatures from 50 to 170 °C in step of 30°C were used in the protocol. The residual doses for the MET-pIRIR signals were generally less than 1 Gy. This protocol was further simplified to a three-step pIRIR method, with three stimulation temperatures of 110, 140 and 170°C. It has been shown that these new pIRIR methods can be applied successfully to aeolian samples within the Holocene.

A high temperature MET-pIRIR dating protocol was initially applied to polymineral fine grains (4-11 µm), recovered from Chinese loess samples collected at Luochuan that accumulated within the last glacial-interglacial period. The MET-pIRIR ages for fine grains were compared with the coarse grain (63-90 µm) K-feldspar MET-pIRIR ages and the coarse grain quartz OSL ages, and the stratigraphic age controls. The results show that the MET-pIRIR protocol can be applied to fine grains from these loess samples without fading correction.

A plateau test, termed the  $D_e(T, t)$  plot, was proposed as a self-diagnosing tool for the pIRIR dating protocols. The pattern of the  $D_e(T, t)$  plot was shown to be affected by non-bleachable signal, partial bleaching and anomalous fading effects. The achievement of a plateau in the  $D_e(T, t)$  plot indicates that the non-fading signal has been achieved, and the effects of non-bleachable dose and partial bleaching are negligible. The  $D_e(T, t)$  test was successfully applied to different pIRIR protocols.

A series of loess and fluvial sand samples were collected from the north piedmont of Tian Shan range to determine appropriate dating procedures for samples in this area. Luminescence properties of quartz and K-feldspar grains extracted from these samples were investigated. The extent of bleaching for the samples and the reliability of the measured ages were assessed based on equivalent dose distribution and age comparison between chronometers. Optimized dating procedures for samples in north Tian Shan have been proposed. K-feldspar MET-pIRIR dating is recommended for the loess samples, while single aliquot quartz OSL dating is suggested for the fluvial sand samples, after consideration of signal brightness and the extent of signal resetting.

The dating procedures proposed above were applied to the deformed fluvial terraces of Anjihai River in the north flank of Tian Shan. Combined with topographic measurements, the deformation rate of the Anjihai anticline was evaluated. The average shortening rates of the Anjihai anticline since 3.6 ± 0.1, 9.0 ± 0.6 and 53.3 ± 2.2 ka were calculated to be 1.4 ± 0.3, 1.2 ± 0.3 and 0.5 ± 0.1 mm/a, respectively. It suggests that the northern Tian Shan region was tectonically active during the late Quaternary, especially in the Holocene.

**Author:** Sebastian Kreutzer  
**Thesis Title:** Luminescence dating of heated silex – Potential to improve accuracy and precision and application to Paleolithic sites  
**Grade:** Ph.D.  
**Date:** August 2012  
**Supervisors:** Alexandra Hilgers, Ulrich Radtke  
**Address:** Institute for Geography, University of Cologne, Otto-Fischer-Str. 4, 50674 Köln, Germany

Understanding morphological processes that sculpt former terrestrial landscapes is one of the driving rationales in Quaternary research. Loess records have been found to be valuable archives for reconstructing paleoenvironmental conditions. However, once identified, characterised and classified by fieldwork, the stratigraphic significance of such records has to be revealed by numerical dating. Luminescence dating, especially optically stimulated luminescence (OSL), is the leading dating approach for establishing chronologies on loess archives. Furthermore, the development of luminescence dating techniques on sediments is closely connected with the history of loess research and vice versa.

As part of the European loess belt the Saxonian Loess Region is located in a transition zone between oceanic dominated western and continental dominated eastern climates. The Saxonian Loess Region comprises up to 20 m thick Weichselian loess accumulations, with intercalated paleosols. For the first time, during the work on this thesis, high-resolution numerical chronologies were established in the Saxonian Loess Region on five loess sections using OSL dating on quartz separates. The dating was employed as a comparison of three quartz grain size fractions commonly used for luminescence dating: (1) coarse (90–200 µm), (2) middle (38–63 µm) and (3) fine grain (4–11 µm). As a survey on four loess sections, three from Germany (Saxony and Saxony-Anhalt) and one from the Czech Republic, these studies investigate the question whether the use of different grain size fractions from one sample yield consistent luminescence characteristics and age results. In summary, seven studies are presented along with an extended summary.

Four studies present numerical chronologies using OSL dating techniques on different grain size and (mineral) fractions. Two studies deal with technical issues that arose during the dating applications. Firstly, an R package for luminescence dating data analysis ('Luminescence') was developed and

secondly, the cross-bleaching behaviour of IR-LEDs of Risø luminescence readers were quantified. One study treats the question whether the common practice of using an identical alpha-efficiency ( $a$ -value) for the conventional IR50 and pIRIR225 dating is justified under theoretical and empirical viewpoints. It was found that for the established numerical chronologies on loess the fine grain quartz fraction results in reliable age estimates up to the Eemian (MIS 5e, 5d). The high-resolution dating in Saxony uncovered a prominent hiatus of ca. 30 ka between the early and the late Weichselian found in all investigated loess sections in Saxony. The fine grain quartz age results are confirmed by the polymineral fine grain dating. For lower dose ranges ( $D_e < 100$  Gy) age results of all three grain size fractions agree within uncertainties. However, the coarse and middle grain fractions show highly scattered distributions. For higher doses ( $D_e > 180$  Gy) the luminescence signals of the coarse and middle grain fractions are in saturation. In contrast, the luminescence signal of the fine grain fraction still grows and is reproducible as shown by test measurements.

The results of a cross-bleaching survey on 10 luminescence readers revealed substantial cross-bleaching behaviour of the IR-LEDs (mean cross-bleaching: ca. 0.026 %), which is an order of magnitude higher than for blue LEDs. The investigation on the  $a$ -values of polymineral fine grain samples gave evidence for significant differences between the mean  $a$ -values obtained with the IR50 and the pIRIR225 signals. The  $a$ -value obtained with the pIRIR225 signal was found to be always higher, but further investigations are needed.

A PDF of this thesis can be downloaded from:  
<https://epub.uni-bayreuth.de/1673>

**Author:** Jillian Moffatt  
**Thesis Title:** Testing the TT-OSL Single-Aliquot Protocol for Quartz Sediment Dating  
**Grade:** Masters  
**Date:** June 2014  
**Supervisors:** Nigel A. Spooner and Barnaby W. Smith  
**Address:** Institute for Photonics and Advanced Sensing (IPAS), School of Chemistry and Physics, University of Adelaide, Australia

Thermally-transferred optically stimulated luminescence (TT-OSL) is a form of optically

stimulated luminescence that saturates at much higher doses than conventional OSL (Wang et al, 2006b). Luminescence sediment dating is a technique whereby the natural radiation dose given to a sample is measured. This is divided by the environmental radiation rate of the sample site to give the sample's age. As TT-OSL is able to measure higher doses than conventional OSL, it has been considered a candidate for long range luminescence sediment dating, beyond one million years. In this thesis, TT-OSL single-aliquot sediment dating protocols were tested on selected samples from the south-east of South Australia (SESA) stranded dune sequence, a sequence of ancient dunes ranging from 0 to 900 thousand years of age that have previously been independently dated using luminescence and non-luminescence dating methods. A young sample with a high natural dose from Baldina Creek, Burra, South Australia was also dated. Measurements of the thermal depletion of the TT-OSL signal were also made.

It was found that, for the SESA samples, TT-OSL dating results do not agree with previous independent measurements above 200 ka. The results for the young Baldina Creek sample were within the expected range.

**Author:** Muhammed Zeynel Öztürk  
**Thesis Title:** Quaternary Geomorphology of North Cyprus Coasts (between Cape Kormakiti-Cape Apostolos Andreas-Cape Elea)  
**Grade:** Ph.D.  
**Date:** May 2013  
**Supervisor:** Dr. Ahmet Evren ERGİNAL  
**Address:** Department of Geography, Niğde University, TR-51240, Niğde, Turkey

Cyprus Island located in the Eastern Mediterranean has strongly been affected by tectonic activities resulting from plate movements, and the uplift of the island continues at the present. The Island has also been affected by the Late Quaternary and Holocene climatic and sea level changes. These changes have had great impacts on the development of the coastal geomorphology. Proofs of these changes are preserved in the beach rocks, marine deposits, wave-cut platforms and eolianites that formed along the coastline. Beachrocks in 23 localities, fossiliferous marine deposits in 3 localities, eolianites in 3 localities, wave-cut platforms in 5 localities were investigated at NCTR coasts in this thesis. Based on

the analysis of the samples collected from the above mentioned localities, the significance of these forms were investigated in terms of the geochemical, geostatistical and dating studies to evaluate the Late Quaternary and Holocene climatic changes, sea level fluctuations and tectonic controls.

The dip direction measurements from the eolianite beds indicate that the paleo wind directions are in accordance with present day wind characteristics. Thus, prevailing wind directions in the Eastern Mediterranean have not showed any significant changes since the formation of the eolianites in Late Quaternary. The ages of the beach rocks, based on the OSL datings, are between  $0.442 \pm 0.079$  and  $5990 \pm 0.341$  BP. These beach rocks were formed in both intertidal and supratidal environments as recognized by calcitic cement types such as meniscus bridge, dogtooth, pore filling and micritic envelopes. Sea level curve shows that beach rocks were formed in two successive rising sea level periods that occurred in a low sea level condition between 0 m and -1m. At present these beach rocks are found well above the mean present sea level despite the fact they formed at 0 and -1 meters. This implies that the tectonic uplift is greater than sea level rise in North Cyprus and this tectonic uplift has occurred at a rate of 0.04 mm/year over the past 6000 years. As the results are compared with the beach rocks studies carried out at the southern coasts of Turkey, it is suggested that a considerable uplift has occurred in the Cilicia-Adana Basin, which is bordered by Misis-Kyrenia Fault Zone. Based on the analyses carried out on wave-cut platforms it is noted that, despite the considerable uplift in the area, the rates of uplift differs locally along the North Cyprus.

**Author:** René Rojas Rocca  
**Thesis Title:** Study of luminescent centers of quartz crystals applied to sediment dating by using Optically Stimulated Luminescence.  
**Grade:** Ph.D.  
**Date:** December 2012  
**Supervisor:** Sonia Hatsue Tatumi  
**Address:** Physics Institute of São Paulo University, São Paulo, Brazil. (Present address: Marine Science Department, Federal University of São Paulo, São Paulo, Brazil.)

The principal aim of the presented work is to study the Thermoluminescence (TL) and Optically Stimulated Luminescence (OSL) of quartz crystals obtained from sediments located at the coast of the state of Maranhão. The analysis of OSL and TL properties was carried out after gamma and beta irradiation, pre-heating, and exposure of samples to solar radiation, having in mind the dating of these sediments. EPR measurements were performed to investigate the possible paramagnetic centers in the sample, as well as establishing some correlation with the OSL and TL centers.

Measurements of single grain dating showed an unexpected behaviour. This result could be evidence that the centers responsible for TL and OSL are not the same. Ages obtained by OSL depend only on the brightest grains, while ages obtained by TL depend on the contribution of multiple grains. The XRD measurements carried out at LNLS confirmed that all the separated grains were quartz grains, although different grains produced different OSL emission, suggesting that these properties are related to different intrinsic point defects and impurities in the grains. EPR signals were measured for quartz grains, using a microwave power of 0.161 mW. It was possible to isolate the signal of the E'1-center. This signal is known to increase from 120 to 300 °C and decreases by treatment beyond 300 °C up to 450 °C and may be related to the TL peaks at high temperatures. ESR measurements at 77 K showed the presence of Al centers. Annual Dose values were found to be between 0.7 to 3.0 mGy/year, and for some profiles the values were more constant (Location B: 1.77 to 1.95 mGy/year). The ages obtained with OSL and TL and the MAR protocol are quite similar, although those obtained by OSL usually are somewhat smaller than the ages obtained by TL. The stratigraphic depths of sediments are directly proportional to the ages obtained. The three ages of the second profile are within the Pleistocene, while the other profiles show ages starting in the Late Pleistocene to Holocene.

A PDF of this thesis can be downloaded from <http://www.teses.usp.br/teses/disponiveis/43/43134/td-27032013-135335/es.php>

**Author:** Rajendra Shrestha  
**Thesis Title:** Optically Stimulated Luminescence (OSL) dating of aeolian sediments of Skåne, South Sweden  
**Grade:** Masters  
**Date:** 2013  
**Supervisors:** Helena Alexanderson and Charlotte Sparrenbom  
**Address:** Rajendra Shrestha, Department of Geology, Lund University, Sölvegatan 12, SE-223 62 Lund, Sweden.

Wind is an important agent of transportation of sediments and to change the landscape. Aeolian sediments can be inferred as a proxy for past climate. In Sweden aeolian sediments are not widespread and there are not so many studies on chronological and paleoenvironmental aspects. It is believed that aeolian sediments were deposited right after deglaciation and reactivated during recent times as a result of human impact and climatic deterioration. For this study, cover sand in Blentarp, south Sweden was selected. Twelve samples for OSL measurement, two samples for  $^{14}\text{C}$  and ten samples for grain size analysis were collected. The main aim of this study was to determine the timing of aeolian sand deposition and to relate it with past climate and environment. A widely accepted chronological technique for aeolian sediment, Optically Stimulated Luminescence (OSL) dating technique was applied to measure the age of the sand deposit. The result from this investigation suggested that there were five episodes of aeolian sedimentation. The oldest event recorded during this study was after deglaciation at ca. 15 200 a. The second episode was at ca. 14 500 to 13 000 a and the last date obtained in this event is at the beginning of the Younger Dryas. The third episode of deposition was at ca. 1900 -1700 a at the time of the Roman warm period. Fourth episode was at ca. 400 -300 a and the fifth or latest episode was at ca. 200 -160 a at the time of the Little ice age. The first episode was deposited right after deglaciation and the remaining four episodes were deposited probably due to climatic impact such as strong storminess or by human activities.

**Keywords:** *Skåne, South Sweden, Vomb basin, Aeolian, Sediments, Grain size, Luminescence, OSL, Chronology*

**Author:** Lauren M. Simkins  
**Thesis Title:** Antarctic raised beaches: Insight on geochronology, relative sea level, and coastal processes  
**Grade:** Ph.D.  
**Date:** September 2014  
**Supervisors:** Alexander R. Simms, Regina DeWitt  
**Address:** Department of Earth Science, University of California Santa Barbara, 1006 Webb Hall, Santa Barbara, California USA, 93106 (Present address: Department of Earth Science, Rice University, 6100 Main Street, Houston, Texas USA, 77005)

Beaches are preserved above sea level along ice-free portions of the Antarctic coastline due to post-glacial rebound associated with glacial isostatic adjustment since the Last Glacial Maximum. The ages and elevations of these beaches provide relative sea-level constraints for glacial isostatic adjustment models and ice-sheet histories. Due to harsh field conditions and difficulty dating Antarctic materials, a lack of geochronological constraints on raised beaches limits our understanding of relative sea level around Antarctica. The focus of the studies discussed here is on Antarctic raised beaches with goals to improve the methods of dating cobble surfaces from raised beaches using optically stimulated luminescence and use the dated beaches to reconstruct relative sea level and better understand Antarctic coastal processes throughout the Holocene. Through a series of cleaning methods applied to sample carriers used for optically stimulated luminescence measurements of sediment, the contamination of dose-dependent, variable signals from sample carriers previously assumed to have neutral signals is eliminated. An analysis of optically stimulated luminescence characteristics of quartz from cobble surfaces with sample petrology and cathodoluminescence provides insight on the suitability of Antarctic materials for optically stimulated luminescence dating. The limited amount of quartz (<10%) found in the majority of the samples often occurs as intergrowths in feldspars characterized by irregular, anhedral crystal form. A lack of discernible relationship between optically stimulated luminescence and cathodoluminescence properties and petrology suggest that cathodoluminescence behavior and petrology are not responsible for the poor luminescence characteristics observed from quartz extracted from cobble surfaces. A relative sea-level history of Marguerite Bay,

Antarctic Peninsula derived from optically stimulated luminescence-dated beach cobble surfaces further constrains post-glacial rebound since the Last Glacial Maximum. New ages suggest the Holocene marine limit for Marguerite Bay is 21.7 masl with an age of ~ 5.5-7.3 ka. Our favored hypothesis for the ages of the beaches from 21.7-40.8 masl at Calmette Bay is that the beaches formed prior to the Last Glacial Maximum. The temporal distribution of circum-Antarctic raised beaches throughout the Holocene is utilized to determine the relationship between wave-energy, sea ice, and coastal evolution. The distribution of raised beaches throughout the Holocene around Antarctica shows synchronous periods of beach formation in the Antarctic Peninsula and the Ross Sea centered at 2.0, 3.5, and 5.3 ky BP while East Antarctic (outside of the Ross Sea) beach formation is out-of-phase with the rest of Antarctica at 3.2, 4.2, 5.8, and 6.5 ky BP. The distribution of beaches in the South Shetland Islands is dominated by enhanced beach formation between 0.2 and 0.7 ky BP most likely due to rapid post-glacial rebound associated with the Little Ice Age with minor peaks in beach formation from 1.3-2.2, 5.1-5.6, and 6.0-6.5 ky BP. Beach formation results from higher wave exposure during periods of reduced sea ice observed from comparison with Holocene sea-ice proxies. The anti-phasing of beach formation in the Antarctic Peninsula and Ross Sea compared to East Antarctica is markedly similar to the phasing of modern and Holocene climate forcing around Antarctica. The findings of these studies focused on Antarctic raised beaches have implications for understanding sea-level, glacial isostatic adjustment, ice-sheet histories, and coastal processes since the Last Glacial Maximum.

Contact L.M. Simkins for a copy of the dissertation at [lsimkins@rice.edu](mailto:lsimkins@rice.edu) or download from Ancient TL.

**Author:** Rachel K Smedley  
**Thesis Title:** Testing the use of single grains of K-feldspar for luminescence dating of proglacial sediments in Patagonia  
**Grade:** Ph.D.  
**Date:** November 2014  
**Supervisors:** Geoff A.T. Duller, Neil F. Glasser  
**Address:** Department of Geography and Earth Sciences, Aberystwyth University, UK

In recent years single-grain dating of quartz has been used to provide luminescence ages of proglacial sediments but the poor sensitivity of the optically stimulated luminescence (OSL) signal of quartz can make dating in some geographical regions challenging. The main aim of this study is to improve luminescence dating in glacial environments by developing and testing methods of single-grain dating of K-feldspars from proglacial sediments using the post-IR infra-red stimulated luminescence (pIRIR) signal. The Lago Buenos Aires valley in Patagonia was chosen as the study site because the existing chronology in the valley that constrains the ages of moraine deposition provides a rare opportunity to compare luminescence dating of proglacial sediments with ages determined using independent dating techniques.

A number of challenges associated with single-grain luminescence dating of K-feldspar are addressed in this study in order to provide accurate ages using the technique. This includes developing a procedure using laser ablation inductively coupled plasma mass spectrometry (LA-ICP-MS) to directly measure the internal K-content of individual grains of K-feldspar, and provide an average internal K-content appropriate for single-grain dating where geochemical measurements of individual grains are not available. Experiments are also performed in this study to demonstrate that the reproducibility of single-grain pIRIR luminescence measurements can be optimised by reducing the disc location temperature from an elevated temperature to room temperature and using the IR LEDs to bleach the grains during the SAR cycle. Laboratory bleaching experiments also demonstrate that the bleaching potential of the pIRIR signal is not expected to be a barrier for single-grain dating of samples in this study.

Finally, IRSL ages are provided for single grains of K-feldspar from two aeolian dune sand samples that were taken from above and below the Kawakawa tephra from North Island, New Zealand, and for a suite of ten proglacial samples from the Lago Buenos Aires valley that are associated with the deposition of moraine ridges dated using cosmogenic isotope dating and  $^{40}\text{Ar}/^{39}\text{Ar}$  dating. The ages ranging from 15 – 111 ka presented in this study agree with the independent numerical age control within dating uncertainties. Therefore, this study suggests that the technique can be used to provide accurate ages for aeolian and proglacial sediments.

**Author:** Ruochen Wang  
**Thesis Title:** Optical Dating of Young Lacustrine Sediment from Lake Manas in Northwestern China  
**Grade:** Masters  
**Date:** August 2014  
**Supervisor:** Sheng-Hua Li  
**Address:** University of Hong Kong

Manas Lake is a closed and dried lake in the Junggar Basin with catchment area of 11,000 square kilometers. The lake is particularly sensitive and important to the study of paleo-climate changes, because the climate in the catchment area is dominantly influenced by the Westlies. Dating of lake paleo-shorelines and lacustrine sediments can provide chronological evidence of water level and climate changes. No evidence for Holocene high lake level was found by previous studies.

The ages of samples were determined using Optically Stimulated Luminescence methodologies. The slope method was used for the determination of the equivalent dose of quartz. Series of Lx and Tx from a number of aliquots for each regenerative dose are analysed to obtain an averaged slope value of the Lx/Tx, by separately fitting Lx-Tx plots under each regenerative dose. In this thesis, the slope method was tested for a series of young lacustrine sediment. It is found that using the slope method can save 40% of the time used needed the conventional SAR procedure. The errors were reduced by measuring a large number of natural aliquots. This approach can effectively improve the reliability of optical dating. It is preferred for dating of young samples, because of weak signals and poor precision.

Fifteen lacustrine sediments and shoreline deposits were dated. These samples were from a borehole, a profile section and shoreline deposits of the latest high lake level. High-resolution data were achieved by using the slope method of OSL signals from quartz for the lacustrine sediments. Magnetic susceptibility of these samples was measured as a proxy for revealing paleo-climate changes. The OSL ages suggested that the lake had experienced a rapid deposition process during 200~600 years ago. Such ages agreed well with the ages of the last high lake level, which was the age of the little ice age. It is concluded that the paleo-climate of Lake Manas was cold and wet during the little ice age. Sedimentation gaps with age gap of 70ka were found between sediments of the little ice age and sediments beneath, from both the lacustrine borehole and paleo-shorelines. It implies that Lake Manas probably drained for a considerable time.

**Author:** Yali Zhou  
**Thesis Title:** Climate changes in the Mu Us and Otindag sand fields (north China) during the late Quaternary: An investigation based on optically stimulated luminescence dating and multi-proxy indicators  
**Grade:** Ph.D.  
**Date:** July 2008  
**Supervisors:** Huayu Lu and Joseph A. Mason  
**Address:** Institute of Earth Environment, Chinese Academy of Sciences, Department of Geography, University of Wisconsin-Madison, USA

The dune system in the Mu Us and Otindag sand fields of northern China is sensitive to climate change, where the local climate is controlled by the East Asian monsoon. It is one of the key sites to investigate the history of past environmental changes in China. Alternating sandy loam soils with sand layers in these sand fields indicate multiple intervals of dune activity and stability. In this study, twenty-one representative sand-sandy soil-sandy loess sections from the Mu Us and Otindag sand fields are investigated with optically stimulated luminescence (OSL) dating to establish the chronology of wet-dry climate variations during the Late Quaternary. On basis of 66 OSL ages and the proxies of grain size distribution, magnetic susceptibility, organic matter content, organic  $\delta^{13}\text{C}$  value and Zr/Rb ratio from more than 300 samples, which are directly related to the climate variations, we refine the regional wet-dry changes and the warm-cold events in the past circa 60 ka.

The equivalent doses (De) were determined by the single aliquot regeneration (SAR) protocol with 90-125 (150)  $\mu\text{m}$  pure quartz particles. The OSL dating results provide a relatively complete and well-dated chronology for wet and dry variations from 57.1 ka to 0 ka. To some extent, the limitations of previous chronology are overcome.

Comparison of the grain-size distribution ( $>63 \mu\text{m}$ ), the magnetic susceptibility and the total organic matter show that the latter two are positively related, and both are negatively related to the coarse grain-size ( $>63 \mu\text{m}$ ) fraction. High sand ( $>63 \mu\text{m}$ ) content is considered to be a direct indicator of the dunes' activity, while the total organic matter and the magnetic susceptibility are indicative of stable dunes. Furthermore, the total organic matter is more sensitive to climate change, especially wet-dry changes, than the magnetic susceptibility. Although

the stable carbon isotopes in soil organic matter (SOCI) can be used as a proxy index of intensity of the summer Asian monsoon in two sand fields, the SOCI variation within plants using a single photosynthetic pathway must be taken into account, especially when the vegetation is pure C<sub>3</sub> plants. Our study indicates that there is no linear relationship between SOCI and the summer monsoon intensity. Zr/Rb ratio, which is positively related to the coarse grain-size (>63 $\mu$ m) fraction and the mean particle size in the Mu Us sand field, may serve as a proxy index of the strength of the East Asian winter monsoon. However, this is limited to the Otindag sand field due to the difference of source rocks.

In the Otindag sand field, the widespread dune mobilization occurred at 17.7ka; from 9.9 ka to 8.2 ka, it was a dry climate. The dunes were mainly stabilized between 8.0 ka and 2.7 ka, implying a relatively wet climate, although there were short-term penetrations of dune activity during this wet period. After ~2.3 ka, the region became dry again, as inferred from widespread dune activity. The “8.2ka” cold event and the Little Ice Age climatic deterioration are detected on the basis of the dune records and OSL ages. During the Medieval Warm Period and the Sui-Tang Warm Period, climate in Otindag sand field was relatively humid and the vegetation was denser, and the sand dunes were stabilized again.

In the Mu Us sand field, the climate was relatively dry between 57.1 and 52.5 ka and the dune system was active. Sandy loess deposition occurred at around 41.2 ka and 37.7 ka, indicates the climate was relative humid and the sand dunes were in the relative stable condition. During the episode of 13.7 and 12.7 ka, coarse sand layers were deposited again, climate was relatively drought-prone, vegetation cover decreased, and the sand field expanded. It was humid as sandy soil developed at 11.6 ka. During the interval of 10.97- 8.67 ka, the total organic matter and the lithology show wet-dry alternate frequently, but the sandy dunes are still mainly active. The Holocene Optimum was revealed from 8.5-2.4 ka, the sandy soil was widely formed in this time. The uppermost aeolian sand layers yielded OSL ages of 0.15 and 0 ka respectively, suggesting the dunes are mobilized in modern times. Some abrupt environment changes, such as H5, Younger Dryas and MIS3 climatic events, were found in the Mu Us sand field.

These aeolian records reveal the climate changes at millennial time scales during the Late Quaternary in the two sand fields, and these climatic changes may be linked to climate variation elsewhere in the Northern Hemisphere, through atmospheric circulation.

Keywords: *OSL dating, Late Quaternary, Mu Us sand field, Otindag sand field, climate change*

## Bibliography

### Compiled by Daniel Richter

---

#### From 1<sup>st</sup> June to 1<sup>th</sup> November 2014

- Abafoni, J. D., Arabi, A. S., and Funtua, I. I. (2014). Luminescence chronology of the Bama Beach Ridge, Chad Basin, north eastern Nigeria. *Quaternary International* **338**, 42-50.
- Andreucci, S., Panzeri, L., Martini, I. P., Maspero, F., Martini, M., and Pascucci, V. (2014). Evolution and architecture of a west mediterranean upper pleistocene to holocene coastal apron-fan system. *Sedimentology* **61**, 333-361.
- Anjar, J., Adrielsson, L., Larsen, N. K., Möller, P., and Barth, K. (2014). Weichselian history of the Fennoscandian ice sheet in southern Sweden and the southwestern Baltic Basin. *Boreas* **43**, 608-626.
- Argyilan, E. P., Lepper, K., and Thompson, T. A. (2014). Late Holocene coastal development along the southern shore of Lake Michigan determined by strategic dating of stabilized parabolic dunes and wetlands of the Tolleston Beach. *Coastline and Dune Evolution Along the Great Lakes* **508**, 31-46.
- Arsuaga, J. L., Martínez, I., Arnold, L. J., Aranburu, A., Gracia-Téllez, A., Sharp, W. D., Quam, R. M., Falguères, C., Pantoja-Pérez, A., Bischoff, J., Poza-Rey, E., Parés, J. M., Carretero, J. M., Demuro, M., Lorenzo, C., Sala, N., Martínón-Torres, M., García, N., Alcázar de Velasco, A., Cuenca-Bescós, G., Gómez-Olivencia, A., Moreno, D., Pablos, A., Shen, C.-C., Rodríguez, L., Ortega, A. I., García, R., Bonmatí, A., Bermúdez de Castro, J. M., and Carbonell, E. (2014). Neandertal roots: Cranial and chronological evidence from Sima de los Huesos. *Science* **344**, 1358-1363.
- Aubry, T., Dimuccio, L. A., Buylaert, J.-P., Liard, M., Murray, A. S., Thomsen, K. J., and Walter, B. (2014). Middle-to-Upper Palaeolithic site formation processes at the Bordes-Fitte rockshelter (Central France). *Journal of Archaeological Science* **52**, 436-457.
- Backwell, L. R., McCarthy, T. S., Wadley, L., Henderson, Z., Steininger, C. M., Bonita, d., Barré, M., Lamothe, M., Chase, B. M., Woodborne, S., Susino, G. J., Bamford, M. K., Sievers, C., Brink, J. S., Rossouw, L., Pollarolo, L., Trower, G., Scott, L., and d'Errico, F. (2014). Multiproxy record of late Quaternary climate change and Middle Stone Age human occupation at Wonderkrater, South Africa. *Quaternary Science Reviews* **99**, 42-59.
- Basak, B., Srivastava, P., Dasgupta, S., Kumar, A., and Rajaguru, S. N. (2014). Earliest dates and implications of microlithic industries of late pleistocene from Mahadebbera and Kana, Purulia district, West Bengal. *Current Science* **107**, 1167-1171.
- Basilici, G., and Dal' Bó, P. F. F. (2014). Influence of subaqueous processes on the construction and accumulation of an aeolian sand sheet. *Earth Surface Processes and Landforms* **39**, 1014-1029.
- Bates, M. R., Wenban-Smith, F. F., Bello, S. M., Bridgland, D. R., Buck, L. T., Collins, M. J., Keen, D. H., Leary, J., Parfitt, S. A., Penkman, K., Rhodes, E., Ryssaert, C., and Whittaker, J. E. (2014). Late persistence of the Acheulian in southern Britain in an MIS 8 interstadial: evidence from Harnham, Wiltshire. *Quaternary Science Reviews* **101**, 159-176.
- Beerten, K., Vandersmissen, N., Deforce, K., and Vandenberghe, N. (2014). Late Quaternary (15 ka to present) development of a sandy landscape in the Mol area, Campine region, north-east Belgium. *Journal of Quaternary Science* **29**, 433-444.
- Bennett, M. R., Morse, S. A., Liutkus-Pierce, C., McClymont, J., Evans, M., Crompton, R. H., and Francis Thackeray, J. (2014). Exceptional preservation of children's footprints from a Holocene footprint site in Namibia. *Journal of African Earth Sciences* **97**, 331-341.
- Bertran, P., Andrieux, E., Antoine, P., Coutard, S., Deschodt, L., Gardère, P., Hernandez, M., Legentil, C., Lenoble, A., Liard, M., Mercier, N., Moine, O., Sitzia, L., and Van Vliet-Lanoë, B. (2014). Distribution and chronology of Pleistocene permafrost features in France: Database and first results. *Boreas* **43**, 699-711.

- Billy, J., Robin, N., Hein, C. J., Certain, R., and FitzGerald, D. M. (2014). Internal architecture of mixed sand-and-gravel beach ridges: Miquelon-Langlade Barrier, NW Atlantic. *Marine Geology* **357**, 53-71.
- Blakemore, A. G., Murray-Wallace, C. V., and Lachlan, T. J. (2014). First recorded evidence of subaqueously-deposited late Pleistocene interstadial (MIS 5c) coastal strata above present sea level in Australia. *Marine Geology* **355**, 377-383.
- Blewett, W. L., Drzyzga, S. A., Sherrod, L., and Wang, H. (2014). Geomorphic relations among glacial Lake Algonquin and the Munising and Grand Marais moraines in eastern Upper Michigan, USA. *Geomorphology* **219**, 270-284.
- Bouvier, A., Reynaud, J.-F., Guibert, P., and Sapin, C. (2014). Luminescence dating applied to Saint-Irénée's church (Lyon, France). *Open Journal of Archaeometry* **2**, 10.4081/arc.2014.5259.
- Busschers, F. S., Wesselingh, F. P., Kars, R. H., Versluijs-Helder, M., Wallinga, J., Bosch, J. H. A., Timmer, J., Nierop, K. G. J., Meijer, T., Bunnik, F. P. M., and De Wolf, H. (2014). RADIOCARBON DATING OF LATE PLEISTOCENE MARINE SHELLS FROM THE SOUTHERN NORTH SEA. *Radiocarbon* **56**, 1151-1166.
- Castillo, M., Muñoz-Salinas, E., and Ferrari, L. (2014). Response of a landscape to tectonics using channel steepness indices (ksn) and OSL: A case of study from the Jalisco Block, Western Mexico. *Geomorphology* **221**, 204-214.
- Cawthra, H. C., Bateman, M. D., Carr, A. S., Compton, J. S., and Holmes, P. J. (2014). Understanding Late Quaternary change at the land-ocean interface: a synthesis of the evolution of the Wilderness coastline, South Africa. *Quaternary Science Reviews* **99**, 210-223.
- Chen, R., Zhou, S., Lai, Z., Ou, X., Chen, R., and Deng, Y. (2014). Luminescence chronology of late Quaternary moraines and Last Glacial Maximum equilibrium-line altitude reconstruction from Parlung Zangbo Valley, south-eastern Tibetan Plateau. *Journal of Quaternary Science* **29**, 597-604.
- Chithambo, M. L., and Niyonzima, P. (2014). On isothermal heating as a method of separating closely collocated thermoluminescence peaks for kinetic analysis. *Journal of Luminescence* **155**, 70-78.
- Choi, S.-J., Jeon, J. S., Choi, J.-H., Kim, B., Ryoo, C.-R., Hong, D.-G., and Chwae, U. (2014). Estimation of possible maximum earthquake magnitudes of Quaternary faults in the southern Korean Peninsula. *Quaternary International* **344**, 53-63.
- Chruścińska, A., Cicha, A., Kijek, N., Palczewski, P., Przegiętka, K., and Sulkowska-Tuszyńska, K. (2014). Luminescence dating of bricks from the gothic Saint James Church in Toruń. *Geochronometria* **41**, 352-360.
- Constantin, D., Begy, R., Vasiliniuc, S., Panaiotu, C., Necula, C., Codrea, V., and Timar-Gabor, A. (2014). High-resolution OSL dating of the Costinești section (Dobrogea, SE Romania) using fine and coarse quartz. *Quaternary International* **334-335**, 20-29.
- Davidovich, U., Goldsmith, Y., Porat, R., and Porat, N. (2014). Dating and Interpreting Desert Structures: The Enclosures of The Judean Desert, Southern Levant, Re-Evaluated. *Archaeometry* **56**, 878-897.
- De Sarkar, S., Mathew, G., Pande, K., Phukon, P., and Singhvi, A. K. (2014). Drainage migration and out of sequence thrusting in Bhalukpong, Western Arunachal Himalaya, India. *Journal of Geodynamics* **81**, 1-16.
- Demuro, M., Arnold, L. J., Parés, J. M., Pérez-González, A., Ortega, A. I., Arsuaga, J. L., Bermúdez de Castro, J. M., and Carbonell, E. (2014). New Luminescence Ages for the Galería Complex Archaeological Site: Resolving Chronological Uncertainties on the Acheulean Record of the Sierra de Atapuerca, Northern Spain. *PLoS ONE* **9**, e110169.
- Dimitrova, I., Mitev, K., Boshkova, T., and Georgiev, S. (2013). An approach to study the distribution of radon in natural materials containing radium. In "Nuclear Science Symposium and Medical Imaging Conference (NSS/MIC), 2013 IEEE." pp. 1-5.
- Dong, G., Zhang, F., Ma, M., Fan, Y., Zhang, J., Wang, Z., and Chen, F. (2014). Ancient landslide-dam events in the Jishi Gorge, upper Yellow River valley, China. *Quaternary Research* **81**, 445-451.

- Dreibrodt, S., Lubos, C., Lomax, J., Sipos, G., Schroedter, T., and Nelle, O. (2014). Holocene landscape dynamics at the tell Arslantepe, Malatya, Turkey – Soil erosion, buried soils and settlement layers, slope and river activity in a middle Euphrates catchment. *The Holocene* **24**, 1351-1368.
- Du, J.-H., and Wang, X.-L. (2014). Optically stimulated luminescence dating of sand-dune formed within the Little Ice Age. *Journal of Asian Earth Sciences* **91**, 154-162.
- Dzieduszyńska, D., Petera-Zganiacz, J., Twardy, J., Kittel, P., Moska, P., and Adamiec, G. (2014). Optical dating and sedimentary record from the terrace depositional profile of the Warta River (Central Poland). *Geochronometria* **41**, 361-368.
- Fábián, S. Á., Kovács, J., Varga, G., Sipos, G., Horváth, Z., Thamó-Bozsó, E., and Tóth, G. (2014). Distribution of relict permafrost features in the Pannonian Basin, Hungary. *Boreas* **43**, 722-732.
- Faivre, J. P., Maureille, B., Bayle, P., Crevecoeur, I., Duval, M., Grün, R., Bemilli, C., Bonilauri, S., Coutard, S., Bessou, M., Limondin-Lozouet, N., Cottard, A., Deshayes, T., Douillard, A., Henaff, X., Pautret-Homerville, C., Kinsley, L., and Trinkaus, E. (2014). Middle pleistocene human remains from Tourville-la-Rivière (Normandy, France) and their archaeological context. *PLoS ONE* **9**, e104111.
- Fisher, T. G., Krantz, D. E., Castaneda, M. R., Loope, W. L., Jol, H. M., Goble, R., Higley, M. C., DeWald, S., and Hanson, P. R. (2014). Coastal geology and recent origins for Sand Point, Lake Superior. In "Special Paper of the Geological Society of America." pp. 85-110508.
- Fitzsimmons, K. E., and Hambach, U. (2014). Loess accumulation during the last glacial maximum: Evidence from Urluia, southeastern Romania. *Quaternary International* **334–335**, 74-85.
- Forman, S. L., Tripaldi, A., and Ciccio, P. L. (2014). Eolian sand sheet deposition in the San Luis paleodune field, western Argentina as an indicator of a semi-arid environment through the Holocene. *Palaeogeography, Palaeoclimatology, Palaeoecology* **411**, 122-135.
- Foroutan, M., Meyer, B., Sébrier, M., Nazari, H., Murray, A. S., Le Dortz, K., Shokri, M. A., Arnold, M., Aumaitre, G., Bourlès, D., Keddadouche, K., Solaymani Azad, S., and Bolourchi, M. J. (2014). Late Pleistocene-Holocene right slip rate and paleoseismology of the Nayband fault, western margin of the Lut block, Iran. *Journal of Geophysical Research B: Solid Earth* **119**, 3517-3560.
- Frouin, M., Lahaye, C., Hernandez, M., Mercier, N., Guibert, P., Brenet, M., Folgado-Lopez, M., and Bertran, P. (2014). Chronology of the Middle Palaeolithic open-air site of Combe Brune 2 (Dordogne, France): a multi luminescence dating approach. *Journal of Archaeological Science* **52**, 524-534.
- Fu, X. (2014). The  $D_e(T, t)$  plot: A straightforward self-diagnose tool for post-IR IRSL dating procedures. *Geochronometria* **41**, 315-326.
- Fujita, H. (2014). Application of pulsed optically stimulated luminescence from surface soil to retrospective dosimetry. *Radiation Physics and Chemistry* **104**, 84-87.
- Galli, A., Martini, M., Maspero, F., Panzeri, L., and Sibilgia, E. (2014). Surface dating of bricks, an application of luminescence techniques. *European Physical Journal Plus* **129**, 1-9.
- Galván, B., Hernández, C. M., Mallol, C., Mercier, N., Sistiaga, A., and Soler, V. (2014). New evidence of early Neanderthal disappearance in the Iberian Peninsula. *Journal of Human Evolution* **75**, 16-27.
- Gandini, R., Rossetti, D. d. F., Netto, R. G., Bezerra, F. H. R., and Góes, A. M. (2014). Neotectonic evolution of the Brazilian northeastern continental margin based on sedimentary facies and ichnology. *Quaternary Research* **82**, 462-472.
- Gao, W., Jia, D.-C., Jiang, Q.-G., Li, T.-L., Liu, C.-R., Li, J.-P., and Wang, Z.-G. (2014). ESR age of a Quaternary sedimentary profile in Manjiang, Fusong County, Changbai Mountain region, and its significance. *Quaternary International* **349**, 49-58.
- Gocke, M., Hambach, U., Eckmeier, E., Schwark, L., Zöller, L., Fuchs, M., Löscher, M., and Wiesenberg, G. L. B. (2014). Introducing an improved multi-proxy approach for paleoenvironmental reconstruction of loess–paleosol archives applied on the Late Pleistocene Nussloch sequence (SW Germany). *Palaeogeography, Palaeoclimatology, Palaeoecology* **410**, 300-315.

- Gold, R. D., Briggs, R. W., Personius, S. F., Crone, A. J., Mahan, S. A., and Angster, S. J. (2014). Latest Quaternary paleoseismology and evidence of distributed dextral shear along the Mohawk Valley fault zone, northern Walker Lane, California. *Journal of Geophysical Research: Solid Earth* **119**, 5014-5032.
- Goode, J. K., Burbank, D. W., and Ormukov, C. (2014). Pliocene-Pleistocene initiation, style, and sequencing of deformation in the central Tien Shan. *Tectonics* **33**, 464-484.
- Gozhik, P., Komar, M., Łanczont, M., Fedorowicz, S., Bogucki, A., Mroczek, P., Prylypko, S., and Kusiak, J. (2014). Paleoenvironmental history of the Middle Dnieper Area from the Dnieper to Weichselian Glaciation: A case study of the Maksymivka loess profile. *Quaternary International* **334-335**, 94-111.
- Greenbaum, N., Schwartz, U., Benito, G., Porat, N., Cloete, G. C., and Enzel, Y. (2014). Paleohydrology of extraordinary floods along the Swakop River at the margin of the Namib Desert and their paleoclimate implications. *Quaternary Science Reviews* **103**, 153-169.
- Guérin, G., and Valladas, H. (2014). Cross-calibration between beta and gamma sources using quartz OSL: Consequences of the use of the SAR protocol in optical dating. *Radiation Measurements* **68**, 31-37.
- Guo, L. T., Wang, P., Zhang, K., Sheng, Q., Zhao, H., and Wang, C. (2013). OSL and  $^{14}\text{C}$  ages of the Late Quaternary sediments in the east Pearl River Delta. *Geology in China* **40**, 1842-1849.
- Guo, X., Lai, Z., Sun, Z., Li, X., and Yang, T. (2014). Luminescence dating of Suozi landslide in the Upper Yellow River of the Qinghai-Tibetan Plateau, China. *Quaternary International* **349**, 159-166.
- Hernandez, M., Mercier, N., Rigaud, J.-P., Texier, J.-P., and Delpech, F. (2014). A revised chronology for the Grotte Vaufrey (Dordogne, France) based on TT-OSL dating of sedimentary quartz. *Journal of Human Evolution* **75**, 53-63.
- Higley, M. C., Fisher, T. G., Jol, H. M., Lepper, K., and Martin-Hayden, J. M. (2014). Stratigraphic and chronologic analysis of the Warren Beach, northwest Ohio, USA. *Canadian Journal of Earth Sciences* **51**, 737-749.
- Hilbert, Y. H., White, T. S., Parton, A., Clark-Balzan, L., Crassard, R., Groucutt, H. S., Jennings, R. P., Breeze, P., Parker, A., Shipton, C., Al-Omari, A., Alsharekh, A. M., and Petraglia, M. D. (2014). Epipalaeolithic occupation and palaeoenvironments of the southern Nefud desert, Saudi Arabia, during the Terminal Pleistocene and Early Holocene. *Journal of Archaeological Science* **50**, 460-474.
- Hobo, N., Makaske, B., Wallinga, J., and Middelkoop, H. (2014). Reconstruction of eroded and deposited sediment volumes of the embanked River Waal, the Netherlands, for the period ad 1631–present. *Earth Surface Processes and Landforms* **39**, 1301-1318.
- Huang, S.-Y., Chen, Y.-G., Burr, G. S., Jaiswal, M. K., Lin, Y. N., Yin, G., Liu, J., Zhao, S., and Cao, Z. (2014). Late Pleistocene sedimentary history of multiple glacially dammed lake episodes along the Yarlung-Tsangpo river, southeast Tibet. *Quaternary Research* **82**, 430-440.
- Huang, W.-l., Yang, X.-p., Li, A., Thompson, J. A., and Zhang, L. (2014). Climatically controlled formation of river terraces in a tectonically active region along the southern piedmont of the Tian Shan, NW China. *Geomorphology* **220**, 15-29.
- Hughes, P., Shawcross, W., Sullivan, M., and Spooner, N. (2014). The geoarchaeology of a Holocene site on the Woolshed Embankment, Lake George, New South Wales. *Australian Archaeology*, 24-32.
- Hwang, S., Park, C.-S., Yoon, S.-O., and Choi, J. (2014). Origin and weathering properties of loess-paleosol sequence in the Goseong area on the east coast of South Korea. *Quaternary International* **344**, 17-31.
- Hyttinen, O., Eskola, K. O., Kaakinen, A., and Salonen, V. P. (2014). First direct age determination for the Baltic Ice Lake/Yoldia Sea transition in Finland. *GFF* **136**, 398-405.
- Jain, M., and Bøtter-Jensen, L. (2014). Luminescence Instrumentation. *Defect and Diffusion Forum* **357**, 245-260.
- Jia, L. Y., Zhang, X. J., Yang, D. C., Li, Z. M., Fan, K. F., Gong, C., Chen, J., and Zhang, J. Z. (2014). The formation age of the Hongshi (red rock) Canyon in the Yuntaishan Global Geopark, Henan Province. *Acta Geoscientica Sinica* **35**, 635-642.

- Johnson, M. O., Mudd, S. M., Pillans, B., Spooner, N. A., Fifield, L. K., Kirkby, M. J., and Gloor, M. (2014). Quantifying the rate and depth dependence of bioturbation based on optically-stimulated luminescence (OSL) dates and meteoric  $^{10}\text{Be}$ . *Earth Surface Processes and Landforms* **39**, 1188-1196.
- Kale, V. S., Sengupta, S., Achyuthan, H., and Jaiswal, M. K. (2014). Tectonic controls upon Kaveri River drainage, cratonic Peninsular India: Inferences from longitudinal profiles, morphotectonic indices, hanging valleys and fluvial records. *Geomorphology* **227**, 153-165.
- Kar, R., Chakraborty, T., Chakraborty, C., Ghosh, P., Tyagi, A. K., and Singhvi, A. K. (2014). Morpho-sedimentary characteristics of the Quaternary Matiali fan and associated river terraces, Jalpaiguri, India: Implications for climatic controls. *Geomorphology* **227**, 137-152.
- Kars, R. H., Reimann, T., Ankjærgaard, C., and Wallinga, J. (2014). Bleaching of the post-IR IRSL signal: new insights for feldspar luminescence dating. *Boreas* **43**, 780-791.
- Kemp, J., Pietsch, T. J., and Olley, J. (2014). Digging your own grave: OSL signatures in experimental graves. *Journal of Human Evolution* **76**, 77-82.
- Kenworthy, M. K., Rittenour, T. M., Pierce, J. L., Sutfin, N. A., and Sharp, W. D. (2014). Luminescence dating without sand lenses: An application of OSL to coarse-grained alluvial fan deposits of the Lost River Range, Idaho, USA. *Quaternary Geochronology* **23**, 9-25.
- King, G. E., Sanderson, D. C. W., Robinson, R. A. J., and Finch, A. A. (2014). Understanding processes of sediment bleaching in glacial settings using a portable OSL reader. *Boreas* **43**, 955-972.
- Kinoshita, A., Mayer, E., Ribau Mendes, V., Figueiredo, A. M. G., and Baffa, O. (2014). Electron spin resonance dating of megafauna from Lagoa dos Porcos, Piauí, Brazil. *Radiation Protection Dosimetry* **159**, 212-219.
- Koster, B., and Reicherter, K. (2014). Sedimentological and geophysical properties of a ca. 4000 year old tsunami deposit in southern Spain. *Sedimentary Geology* **314**, 1-16.
- Kreutzer, S., Schmidt, C., DeWitt, R., and Fuchs, M. (2014). The a-value of polymineral fine grain samples measured with the post-IR IRSL protocol. *Radiation Measurements* **69**, 18-29.
- Lasberg, K., Kalm, V., and Kihno, K. (2014). Ice-free interval corresponding to Marine Isotope Stages 4 and 3 at the Last Glacial Maximum position at Kileshino, Valdaj Upland, Russia. *Estonian Journal of Earth Sciences* **63**, 88-96.
- Le Béon, M., Suppe, J., Jaiswal, M. K., Chen, Y.-G., and Ustaszewski, M. E. (2014). Deciphering cumulative fault slip vectors from fold scarps: Relationships between long-term and coseismic deformations in central Western Taiwan. *Journal of Geophysical Research: Solid Earth* **119**, 5943-5978.
- Lewis, S. E., Olley, J., Furuichi, T., Sharma, A., and Burton, J. (2014). Complex sediment deposition history on a wide continental shelf: Implications for the calculation of accumulation rates on the Great Barrier Reef. *Earth and Planetary Science Letters* **393**, 146-158.
- Li, B., Jacobs, Z., Roberts, R., and Li, S.-H. (2014). Review and assessment of the potential of post-IR IRSL dating methods to circumvent the problem of anomalous fading in feldspar luminescence. *Geochronometria* **41**, 178-201.
- Li, G., Dong, G., Wen, L., and Chen, F. (2014). Overbank flooding and human occupation of the Shalongka site in the Upper Yellow River Valley, northeast Tibet Plateau in relation to climate change since the last deglaciation. *Quaternary Research* **82**, 354-365.
- Li, T., Mo, D., Kidder, T., Zhang, Y., Wang, H., and Wu, Y. (2014). Holocene environmental change and its influence on the prehistoric culture evolution and the formation of the Taosi site in Linfen basin, Shanxi province, China. *Quaternary International* **349**, 402-408.
- Li, Y., Wang, N., Zhang, C., and Wang, Y. (2014). Early Holocene environment at a key location of the northwest boundary of the Asian summer monsoon: a synthesis on chronologies of Zhuye Lake, Northwest China. *Journal of Arid Land* **6**, 511-528.
- Li, Z., Xu, Q., Zhang, S., Hun, L., Li, M., Xie, F., Wang, F., and Liu, L. (2014). Study on stratigraphic age, climate changes and environment background of Houjiayao Site in Nihewan Basin. *Quaternary International* **349**, 42-48.

- Link, P. K., Crosby, B. T., Lifton, Z. M., Eversole, E. A., and Rittenour, T. M. (2014). The late pleistocene (17 ka) soldier bar landslide and big Creek Lake, Frank Church-River of no return wilderness, central Idaho, U.S.A. *Rocky Mountain Geology* **49**, 17-31.
- Liu, C.-R., Yin, G. M., Zhou, Y. S., Gao, L., Han, F., and Li, J. P. (2014). ESR studies on quartz extracted from shallow fault gouges related to the Ms 8.0 Wenchuan earthquake - China - Implications for ESR signal resetting in quaternary faults. *Quaternaire* **25**, 67-74.
- Liu, C.-R., Yin, G.-M., Deng, C.-L., Han, F., and Song, W.-J. (2014). ESR dating of the Majuangou and Banshan Paleolithic sites in the Nihewan Basin, North China. *Journal of Human Evolution* **73**, 58-63.
- Liu, X., Fisher, T. G., Lepper, K., and Lowell, T. V. (2014). Geochemical characteristics of glacial Lake Agassiz sediments and new ages for the Moorhead Phase at Fargo, North Dakota, USA. *Canadian Journal of Earth Sciences* **51**, 850-861.
- Lomax, J., Kreutzer, S., and Fuchs, M. (2014). Performance tests using the Lexsyg luminescence reader. *Geochronometria* **41**, 327-333.
- Lovedy Singh, L., and Gartia, R. K. (2014). Glow-curve deconvolution of thermoluminescence curves in the simplified OTOR equation using the Hybrid Genetic Algorithm. *Nuclear Instruments and Methods in Physics Research Section B: Beam Interactions with Materials and Atoms* **319**, 39-43.
- Loveson, V. J., Gujar, A. R., Iyer, S., Udayaganesan, P., Luis, R. A. A., Gaonkar, S. S., Chithrabhanu, P., Tirodkar, G. M., and Singhvi, A. K. (2014). Beach dynamics and oscillations of shoreline position in recent years at Miramar Beach, Goa, India: a study from a GPR survey. *Natural Hazards* **73**, 2089-2106.
- Lu, H., Zhang, T., Zhao, J., Si, S., Wang, H., Chen, S., Zheng, X., and Li, Y. (2014). Late Quaternary alluvial sequence and uplift-driven incision of the Urumqi River in the north front of the Tian Shan, northwestern China. *Geomorphology* **219**, 141-151.
- Lyons, R., Tooth, S., and Duller, G. A. T. (2014). Late Quaternary climatic changes revealed by luminescence dating, mineral magnetism and diffuse reflectance spectroscopy of river terrace palaeosols: a new form of geoproxy data for the southern African interior. *Quaternary Science Reviews* **95**, 43-59.
- Lyså, A., Larsen, E., Buylaert, J.-P., Fredin, O., Jensen, M. A., Kuznetsov, D., Murray, A. S., Subetto, D. A., and van Welden, A. (2014). Late Pleistocene stratigraphy and sedimentary environments of the Severnaya Dvina-Vycheгда region in northwestern Russia. *Boreas* **43**, 759-779.
- Mallinson, D. J., Culver, S. J., Corbett, D. R., Parham, P. R., Shazili, N. A. M., and Yaacob, R. (2014). Holocene coastal response to monsoons and relative sea-level changes in northeast peninsular Malaysia. *Journal of Asian Earth Sciences* **91**, 194-205.
- Marković, S. B., Korač, M., Mrđić, N., Buylaert, J.-P., Thiel, C., McLaren, S. J., Stevens, T., Tomič, N., Petič, N., Jovanović, M., Vasiljević, D. A., Sümegi, P., Gavrilov, M. B., and Obreht, I. (2014). Palaeoenvironment and geoconservation of mammoths from the Nosak loess-palaeosol sequence (Drmno, northeastern Serbia): Initial results and perspectives. *Quaternary International* **334-335**, 30-39.
- Martin, L., Mercier, N., and Incerti, S. (2014). Geant4 simulations for sedimentary grains in infinite matrix conditions: The case of alpha dosimetry. *Radiation Measurements* **70**, 39-47.
- McPherson, A., Clark, D., Macphail, M., and Cupper, M. (2014). Episodic post-rift deformation in the south-eastern Australian passive margin: evidence from the Lapstone Structural Complex. *Earth Surface Processes and Landforms* **39**, 1449-1466.
- Mehta, M., Dobhal, D., Pratap, B., Majeed, Z., Gupta, A. K., and Srivastava, P. (2014). Late Quaternary glacial advances in the Tons River Valley, Garhwal Himalaya, India and regional synchronicity. *The Holocene* **24**, 1336-1350.
- Mena, F., Blanco, J. F., Mariani, F., and Román, A. (2014). Thermoluminescence Dating of Surface Lithic Artefacts from the Chacabuco Valley, Chilean Patagonia. *Archaeometry* **56**, 898-911.
- Meszner, S., Kreutzer, S., Fuchs, M., and Faust, D. (2014). Identifying depositional and pedogenetic controls of Late Pleistocene loess-paleosol sequences (Saxony, Germany) by combined grain size and microscopic analyses. *Zeitschrift für Geomorphologie* **58**, 63-90.

- Mietton, M., Cordier, S., Frechen, M., Dubar, M., Beiner, M., and Andrianaivoarivony, R. (2014). New insights into the age and formation of the Ankarokaroka lavaka and its associated sandy cover (NW Madagascar, Ankarafantsika natural reserve). *Earth Surface Processes and Landforms* **39**, 1467-1477.
- Muñoz-Salinas, E., Bishop, P., Sanderson, D., and Kinnaird, T. (2014). Using OSL to assess hypotheses related to the impacts of land use change with the early nineteenth century arrival of Europeans in south-eastern Australia: an exploratory case study from Grabben Gullen Creek, New South Wales. *Earth Surface Processes and Landforms* **39**, 1576-1586.
- Nian, X., Gao, X., Xie, F., Mei, H., and Zhou, L. (2014). Chronology of the Youfang site and its implications for the emergence of microblade technology in North China. *Quaternary International* **347**, 113-121.
- Nian, X., Gao, X., and Zhou, L. (2014). Chronological studies of Shuidonggou (SDG) Locality 1 and their significance for archaeology. *Quaternary International* **347**, 5-11.
- Nicolay, A., Raab, A., Raab, T., Roesler, H., Boenisch, E., and Murray, A. S. (2014). Evidence of (pre-) historic to modern landscape and land use history near Janschwalde (Brandenburg, Germany). *Zeitschrift für Geomorphologie* **58**, 7-31.
- Orsolya, T., György, S., and Zoltán, H. (2014). TL/OSL kormeghatározás tesztelése római kori bélyeges tégláko / The testing of TL and OSL methods on archeologically accurately dated brick samples. *Archeometriai Műhely* **11**, 13-26.
- Pagonis, V., Gochnour, E., Hennessey, M., and Knowler, C. (2014). Monte Carlo simulations of luminescence processes under quasi-equilibrium (QE) conditions. *Radiation Measurements* **67**, 67-76.
- Pagonis, V., Phan, H., Goodnow, R., Rosenfeld, S., and Morthekai, P. (2014). Mathematical characterization of continuous wave infrared stimulated luminescence signals (CW-IRSL) from feldspars. *Journal of Luminescence* **154**, 362-368.
- Panin, A., Adamiec, G., Arslanov, K., Bronnikova, M., Filippov, V., Sheremetskaya, E., Zaretskaya, N., and Zazovskaya, E. (2014). Absolute chronology of fluvial events in the Upper Dnieper River system and its palaeogeographic implications. *Geochronometria* **41**, 278-293.
- Pederson, J. L., Chapot, M. S., Simms, S. R., Sohbaty, R., Rittenour, T. M., Murray, A. S., and Cox, G. (2014). Age of Barrier Canyon-style rock art constrained by cross-cutting relations and luminescence dating techniques. *Proceedings of the National Academy of Sciences* **111**, 12986-12991.
- Peng, J., Dong, Z., Han, F., Han, Y., and Dai, X. (2014). Estimating the number of components in an OSL decay curve using the Bayesian Information Criterion. *Geochronometria* **41**, 334-341.
- Polymeris, G. S. (2015). OSL at elevated temperatures: Towards the simultaneous thermal and optical stimulation. *Radiation Physics and Chemistry* **106**, 184-192.
- Polymeris, G. S., Kiyak, N. G., Koul, D. K., and Kitis, G. (2014). The Firing Temperature of Pottery from Ancient Mesopotamia, Turkey, Using Luminescence Methods: A Case Study for Different Grain-Size Fractions. *Archaeometry* **56**, 805-817.
- Preusser, F., Muru, M., and Rosentau, A. (2014). Comparing different post-IR IRSL approaches for the dating of Holocene coastal foredunes from Ruhnu Island, Estonia. *Geochronometria* **41**, 342-351.
- Przegietka, K., and Chruscinska, A. (2014). On application of low doses from beta radiation source in OSL retrospective dosimetry. *Radiation Physics and Chemistry* **104**, 118-123.
- Rawling, J. E., III, and Hanson, P. R. (2014). Dune formation on late Holocene sandy bay barriers along Lake Michigan's Door Peninsula: The importance of increased sediment supply following the Nipissing and Algoma high lake-level phases. In "Special Paper of the Geological Society of America." pp. 65-83508.
- Reddy, J. N., and Murthy, K. V. R. (2014). TLD Instrumentation: A Case Study of PC Controlled TL Reader. *Defect and Diffusion Forum* **357**, 261-273.
- Renzelli, D., Pasquale, B., Valentino, P., Federica, S., Rocco, P., Mariano, D., Donatella, B., and Antonino, O. (2013). SAR TL dating of Neolithic and Medieval ceramics from Lamezia, Calabria (South Italy): A case study. *Mediterranean Archaeology & Archaeometry* **13**, 277-288.

- Richter, D., and Krbetschek, M. (2014). Preliminary Luminescence Dating Results for two Middle Palaeolithic Occupations at Neumark-Nord 2. In "Multidisciplinary Studies of the Middle Palaeolithic record from Neumark-Nord (Germany). Volume 1." (S. Gaudzinski-Windheuser, and W. Roebroeks, Eds.), pp. 131-136. Veröffentlichungen des Landesamtes für Denkmalpflege und Archäologie Sachsen-Anhalt. Landesamt für Denkmalpflege und Archäologie Sachsen-Anhalt, Halle.
- Rittase, W. M., Kirby, E., McDonald, E., Douglas Walker, J., Gosse, J., Spencer, J. Q. G., and Herra, A. J. (2014). Temporal variations in Holocene slip rate along the central Garlock fault, Pilot Knob Valley, California. *Lithosphere* **6**, 48-58.
- Roskin, J., Blumberg, D. G., and Katra, I. (2014). Last millennium development and dynamics of vegetated linear dunes inferred from ground-penetrating radar and optically stimulated luminescence ages. *Sedimentology* **61**, 1240-1260.
- Roskin, J., Katra, I., Agha, N., Goring-Morris, A. N., Porat, N., and Barzilai, O. (2014). Rapid anthropogenic response to short-term aeolian-fluvial palaeoenvironmental changes during the Late Pleistocene–Holocene transition in the northern Negev Desert, Israel. *Quaternary Science Reviews* **99**, 176-192.
- Rousseau, D. D., Ghil, M., Kukla, G., Sima, A., Antoine, P., Fuchs, M., Hatté, C., Lagroix, F., Debret, M., and Moine, O. (2013). Major dust events in Europe during marine isotope stage 5 (130-74 ka): a climatic interpretation of the "markers". *Climate of the Past* **9**, 2213-2230.
- Rufer, D., Preusser, F., Schreurs, G., Gnos, E., and Berger, A. (2014). Late Quaternary history of the Vakinankaratra volcanic field (central Madagascar): Insights from luminescence dating of phreatomagmatic eruption deposits. *Bulletin of Volcanology* **76**, 1-20.
- Şahiner, E., Meriç, N., and Polymeris, G. S. (2014). Assessing the impact of IR stimulation at increasing temperatures to the OSL signal of contaminated quartz. *Radiation Measurements* **68**, 14-22.
- Salonen, V.-P., Moreau, J., Hyttinen, O., and Eskola, K. O. (2014). Mid-Weichselian interstadial in Kolari, western Finnish Lapland. *Boreas* **43**, 627-638.
- Santonja, M., Pérez-González, A., Domínguez-Rodrigo, M., Panera, J., Rubio-Jara, S., Sesé, C., Soto, E., Arnold, L. J., Duval, M., Demuro, M., Ortiz, J. E., de Torres, T., Mercier, N., Barba, R., and Yravedra, J. (2014). The Middle Paleolithic site of Cuesta de la Bajada (Teruel, Spain): a perspective on the Acheulean and Middle Paleolithic technocomplexes in Europe. *Journal of Archaeological Science* **49**, 556-571.
- Schiller, M., Dickinson, W., Zondervan, A., Ditchburn, R., and Wang, N. (2014). Rapid soil accumulation in a frozen landscape. *Geology* **42**, 335-338.
- Schmidt, E. D., Tsukamoto, S., Frechen, M., and Murray, A. S. (2014). Elevated temperature IRSL dating of loess sections in the East Eifel region of Germany. *Quaternary International* **334–335**, 141-154.
- Sfampa, I. K., Polymeris, G. S., Tsirliganis, N. C., Pagonis, V., and Kitis, G. (2014). Prompt isothermal decay of thermoluminescence in an apatite exhibiting strong anomalous fading. *Nuclear Instruments and Methods in Physics Research, Section B: Beam Interactions with Materials and Atoms* **320**, 57-63.
- Shao, Q., Wang, W., Deng, C., Voinchet, P., Lin, M., Zazzo, A., Douville, E., Dolo, J.-M., Falguères, C., and Bahain, J.-J. (2014). ESR, U-series and paleomagnetic dating of Gigantopithecus fauna from Chui Feng Cave, Guangxi, southern China. *Quaternary Research* **82**, 270-280.
- Shen, J., Yang, W., Liu, T., Huang, X., Zheng, W., Yu, L., and Wang, G. (2014). Dating fault activity based on surface texture of quartz grains from the Bailong river fault. *Acta Geologica Sinica* **88**, 1131-1144.
- Shi, X., Kirby, E., Lu, H., Robinson, R., Furlong, K. P., and Wang, E. (2014). Holocene slip rate along the Gyaring Co Fault, central Tibet. *Geophysical Research Letters* **41**, 5829-5837.
- Simoës, M., Chen, Y. G., Shinde, D. P., and Singhvi, A. K. (2014). Lateral variations in the long-term slip rate of the Chelungpu fault, Central Taiwan, from the analysis of deformed fluvial terraces. *Journal of Geophysical Research-Solid Earth* **119**, 3740-3766.
- Smith, L. N., and Hanson, M. A. (2014). Sedimentary record of glacial Lake Missoula along the Clark Fork River from deep to shallow positions in the former lakes: St. Regis to near Drummond, Montana. *Exploring the Northern Rocky Mountains* **37**, 51-63.

- Sohn, M. F., Knott, J. R., and Mahan, S. A. (2014). Paleoseismology of the southern section of the Black Mountains and Southern Death Valley Fault zones, Death Valley, United States. *Environmental and Engineering Geoscience* **20**, 177-198.
- Stella, G., Fontana, D., Gueli, A., and Troja, S. (2014). Different approaches to date bricks from historical buildings. *Geochronometria* **41**, 256-264.
- Stevens, T., Jestico, M. J., Evans, G., and Kirkham, A. (2014). Eustatic control of late Quaternary sea-level change in the Arabian/Persian Gulf. *Quaternary Research* **82**, 175-184.
- Stevens, T., Paull, C. K., Ussler, W., III, McGann, M., Buylaert, J. P., and Lundsten, E. (2014). The timing of sediment transport down Monterey Submarine Canyon, offshore California. *Geological Society of America Bulletin* **126**, 103-121.
- Sullivan, M., Hughes, P., Way, A. M., and Spooner, N. (2014). Prehistoric mining at Olympic Dam in arid South Australia. *Archaeology in Oceania* **49**, 43-55.
- Terpiłowski, S., Zieliński, T., Kusiak, J., Pidek, I. A., Czubla, P., Hrynowiecka, A., Godlewska, A., Zieliński, P., and Malek, M. (2014). How to resolve pleistocene stratigraphic problems by different methods? A case study from eastern Poland. *Geological Quarterly* **58**, 235-250.
- Thompson, T. A., Johnston, J. W., and Lepper, K. (2014). The contemporary elevation of the peak Nipissing phase at outlets of the upper Great Lakes. In "Special Paper of the Geological Society of America." pp. 15-29508.
- Toyoda, S., Fujiwara, T., Uchida, A., Ishibashi, J.-i., Nakai, S. i., and Takamasa, A. (2014). ESR dating of barite in sulphide deposits formed by the sea-floor hydrothermal activities. *Radiation Protection Dosimetry* **159**, 203-211.
- Umhoefer, P. J., Maloney, S. J., Buchanan, B., Arrowsmith, J. R., Martinez-Gutiérrez, G., Kent, G., Driscoll, N., Harding, A., Kaufman, D., and Rittenour, T. (2014). Late Quaternary faulting history of the Carrizal and related faults, La Paz region, Baja California Sur, Mexico. *Geosphere* **10**, 476-504.
- Viveen, W., Sanjurjo-Sanchez, J., Goy-Diz, A., Veldkamp, A., and Schoorl, J. M. (2014). Paleofloods and ancient fishing weirs in NW Iberian rivers. *Quaternary Research* **82**, 56-65.
- Wagner, B., Leng, M. J., Wilke, T., Boehm, A., Panagiotopoulos, K., Vogel, H., Lacey, J. H., Zanchetta, G., and Sulpizio, R. (2014). Distinct lake level lowstand in Lake Prespa (SE Europe) at the time of the 74 (75) ka Toba eruption. *Climate of the Past* **10**, 261-267.
- Wang, L., Huang, C. C., Pang, J., Zha, X., and Zhou, Y. (2014). Paleofloods recorded by slackwater deposits in the upper reaches of the Hanjiang River valley, middle Yangtze River basin, China. *Journal of Hydrology* **519**, Part A, 1249-1256.
- Wenxia, H., Zhibang, M., Zhongping, L., Appel, E., Xiaomin, F., and Lupeng, Y. (2014). Wind erosion on the north-eastern Tibetan Plateau: constraints from OSL and U-Th dating of playa salt crust in the Qaidam Basin. *Earth Surface Processes and Landforms* **39**, 779-89.
- Wiwegwin, W., Hisada, K.-I., Charusiri, P., Kosuwan, S., Pailoplee, S., Saithong, P., Khaowiset, K., and Won-In, K. (2014). Paleoearthquake Investigations of the Mae Hong Son Fault, Mae Hong Son Region, Northern Thailand. *Journal of Earthquake and Tsunami* **08**, 1450007.
- Yi, L., Ye, X., Chen, J., Li, Y., Long, H., Wang, X., Du, J., Zhao, S., and Deng, C. (2014). Magnetostratigraphy and luminescence dating on a sedimentary sequence from northern East China Sea: Constraints on evolutionary history of eastern marginal seas of China since the Early Pleistocene. *Quaternary International* **349**, 316-326.
- Yoshizumi, M. T., and Caldas, L. V. E. (2014). TL emission spectra measurements using a spectrometer coupled to the Risoe TL/OSL reader. *Radiation Physics and Chemistry* **104**, 292-296.
- Yu, L., and Lai, Z. (2014). Holocene climate change inferred from stratigraphy and OSL chronology of aeolian sediments in the Qaidam Basin, northeastern Qinghai-Tibetan Plateau. *Quaternary Research* **81**, 488-499.
- Zhang, J., Tsukamoto, S., Grube, A., and Frechen, M. (2014). OSL and <sup>14</sup>C chronologies of a Holocene sedimentary record (Garding-2 core) from the German North Sea coast. *Boreas* **43**, 856-868.

- Zhang, K., Ma, Z., Grapes, R., and Peng, Z. (2014). Asymmetrical river valleys in response to tectonic tilting and strike-slip faulting, northeast margin of Tibetan Plateau. *Earth Surface Processes and Landforms* **39**, 1642-1650.
- Zhang, W., Liu, B., Li, Y., Feng, J., Harbor, J. M., Liu, L., Wang, Z., and Li, D. (2014). Late Pleistocene Glaciations on Qianhu Mountain, Northwest Yunnan Province, China. *Geografiska Annaler: Series A, Physical Geography* **96**, 417-429.
- Zucca, C., Andreucci, S., Akşit, T., Koca, Y. K., Madrau, S., Pascucci, V., Previtali, F., Shaddad, S. M., and Kapur, S. (2014). Buried palaeosols of NW Sardinia (Italy) as archives of the Late Quaternary climatic fluctuations. *Catena* **122**, 72-90.
- Zucca, C., Sechi, D., Andreucci, S., Shaddad, S. M., Deroma, M., Madrau, S., Previtali, F., Pascucci, V., and Kapur, S. (2014). Pedogenic and palaeoclimatic evidence from an Eemian calcrete in north-western Sardinia (Italy). *European Journal of Soil Science* **65**, 420-435.

### Papers from the 2<sup>nd</sup> L.A.I.S. 2012, published in *Mediterranean Archaeology and Archaeometry* **13/3**

- Asfora, V. K., Guzzo, P. L., Pessis, A. M., Watanabe, S., and Khoury, H. J. (2013). Recognizing the burning status of archaeological quartz pebbles coupling thermoluminescence and electron paramagnetic resonance spectroscopy. *Mediterranean Archaeology and Archaeometry* **13**, 127-135.
- Bortolussi, C., Panzeri, L., Sibilìa, E., Zoleo, A., Brustolon, M., Martini, M., Salvatori, S., and Usai, D. (2013). Luminescence and electron paramagnetic resonance properties of prehistoric ceramics from al-khiday excavation site, Sudan. *Mediterranean Archaeology and Archaeometry* **13**, 81-92.
- Galli, A., Martini, M., and Sibilìa, E. (2013). Using the TL pre-dose technique for the TL examination of glass mosaics. *Mediterranean Archaeology and Archaeometry* **13**, 17-24.
- Kim, M. J., Jung, B. G., Kim, S. Y., and Hong, D. G. (2013). Comparison of OSL and 14C dates estimated from Paleolithic paleosol of the Suheol-ri site in Cheonan, Korea. *Mediterranean Archaeology and Archaeometry* **13**, 117-126.
- Kinnaird, T. C., Dixon, J. E., Robertson, A. H. F., Peltenburg, E., and Sanderson, D. C. W. (2013). Insights on topography development in the Vasilikós and Dhiarizos valleys, Cyprus, from integrated OSL and landscape studies. *Mediterranean Archaeology and Archaeometry* **13**, 49-62.
- Liritzis, I., Stamoulis, K., Papachristodoulou, C., and Ioannides, K. (2013). A re-evaluation of radiation dose-rate conversion factors. *Mediterranean Archaeology and Archaeometry* **13**, 1-15.
- Liritzis, I., Vafiadou, A., Zacharias, N., Polymeris, G. S., and Bednarik, R. G. (2013). Advances in surface luminescence dating: New data from selected monuments. *Mediterranean Archaeology and Archaeometry* **13**, 105-115.
- Polymeris, G. S., Kitis, G., Afouxenidis, D., Sfampa, I. K., Tsirliganis, N. C., Rousaki, A., Kouloumpi, E., and Paraskevopoulos, K. M. (2013). On the feasibility of dating portable paintings: Preliminary luminescence measurements on ground layer materials. *Mediterranean Archaeology and Archaeometry* **13**, 93-103.
- Polymeris, G. S., Theodosoglou, E., Kitis, G., Tsirliganis, N. C., Koroneos, A., and Paraskevopoulos, K. M. (2013). Preliminary results on structural state characterization of K-feldspars by using thermoluminescence. *Mediterranean Archaeology and Archaeometry* **13**, 155-161.
- Rodrigues, A. L., Burbidge, C. I., Dias, M. I., Rocha, F., Valera, A., and Prudêncio, M. I. (2013). Luminescence and mineralogy of profiling samples from negative archaeological features. *Mediterranean Archaeology and Archaeometry* **13**, 37-47.
- Sanjurjo-Sanchez, J., Gomez-Heras, M., and Polymeris, G. S. (2013). Estimating maximum temperatures attained during fires in building stoneworks by thermoluminescence: A case study from Uncastillo, Saragossa (Spain). *Mediterranean Archaeology and Archaeometry* **13**, 145-153.
- Sanjurjo-Sánchez, J., and Mato, M. P. (2013). Delimiting the urban growth of Santiago de Compostela (NW Spain) by OSL dating of medieval anthropogenic sediments. *Mediterranean Archaeology and Archaeometry* **13**, 163-173.

- Sfampa, I. K., Polymeris, G. S., Zacharias, N., Kitis, G., and Henderson, J. (2013). Luminescence as a probe in provenance and technological studies of early Islamic raw furnace glasses. *Mediterranean Archaeology and Archaeometry* **13**, 63-69.
- van Nieuland, J., Vandenberghe, D., Gelaude, F., and van den Haute, P. (2013). Absolute dating of aeolian sediments in relationship to the development of the city of Ghent: First results. *Mediterranean Archaeology and Archaeometry* **13**, 25-35.

## Conference Announcements

---

# XIX INQUA 2015

## NAGOYA, JAPAN

### 27 July—2 August, 2015

The next INQUA congress will be held in Nagoya on 27 July - 2 August, 2015. We hope many of the LED participants will not miss this opportunity to visit Japan. Our OSL-ESR session has been approved including other methods such as with cosmogenic nuclei. Please visit the web site

<http://inqua2015.jp/>

and

<http://convention.itbcom.co.jp/inqua2015/session/s08.html>

for the details of the session.

**Deadline for abstract submission:  
Dec. 20, 2014**

**Shin Toyoda**

# Submission of articles to Ancient TL

---

## Reviewing System

In order to ensure acceptable standards and minimize delay in publication, a modification of the conventional refereeing system has been devised for Ancient TL:

Articles can be sent directly by authors to a member of the Reviewers Panel chosen on the basis of the subject matter, but who is not in any of the authors' laboratories. **At the discretion of the Editor**, reviewers who are not listed in the Panel may be used.

The reviewing system aims to encourage direct dialogue between author and reviewer. The Editor should be kept advised of the progress of articles under review by sending him copies of all correspondence. He is available for advice where reviewing difficulties have arisen. Authors whose mother tongue is not English are required to have their manuscript revised for English *before* submitting it.

We ask reviewers to specify (where required) the minimum of revision that is consistent with achieving a clear explanation of the subject of the paper, the emphasis being on *rapid* publication; reviewers are encouraged to make a brief written comment for publication at the end of the paper. Where a contribution is judged not to meet an adequate standard without substantial modification, the author will be advised that the contribution is not suitable for publication. Articles that are not considered to be of sufficient interest may also be rejected.

## Procedures

1. Articles should be submitted to an appropriate member of the Reviewing Panel or Editorial Board, chosen on the basis of the subject matter, but who is not in any of the authors' laboratories.
2. Articles should not normally exceed the equivalent of 5000 words inclusive of diagrams, tables and references. Greater space will be appropriate for certain topics; for these the Editor should first be consulted.  
Short notes and letters are also invited. These should not exceed two printed pages in Ancient TL, including diagrams, tables and references (equivalent to ~1400 words of text).
3. Diagrams and labels should be ready for direct reproduction and not normally exceed 12 cm wide by 10 cm high. Where possible, high quality electronic versions of figures should be submitted. Separate figure captions should be supplied. Inappropriately scaled drawings and labels will be returned for alteration.
4. Authors are asked to submit the paper, including diagrams, to the Reviewer and a duplicate copy to the Editor.  
The final version of the text must be submitted to the Editor electronically using a standard format (Microsoft Word for PC is currently used for producing Ancient TL). Electronic copies of Diagrams and Tables should also be submitted.
5. Upon receipt of an article, the Editor will send an acknowledgement to the author. If the Reviewer is unable to deal with the contribution within **4 weeks** he/she will inform the author and advise the Editor.

## Requirements under various situations

*When agreement concerning an article has been reached:*

The Editor should receive a copy of the final version of the paper, both as hard copy and electronically. The Reviewer should send their final decision, including comments for publication if any, to the Editor.

*If the article has not been rejected, but agreement on its final form cannot be reached or where there are protracted delays in the reviewing process:*

The Editor may request an assessment from the Reviewer and responsibility passes to the Editor.

*If the article is rejected:*

The Editor and author receive notification from the Reviewer, with an indication of the reason for rejection.

**Thesis abstracts** are to be sent to the Editor and in principle do not need reviewing. However, authors are requested to make sure that the English is correct before submission. Thesis abstracts should not exceed 750 words, and figures and tables are not accepted.

**Advertising.** Formal information on equipment can be published in Ancient TL. It should not exceed one printed page. Current charges are displayed on the website (<http://www.ecu.edu/cs-cas/physics/Ancient-TL.cfm>)

## Subscriptions to Ancient TL

Ancient TL Vol. 32 No.2 2014 will be the last issue that is published in print. Future issues will be available for download free of charge from the Ancient TL website (<http://www.ecu.edu/cs-cas/physics/Ancient-TL.cfm>)